

PASCAL



Dep	Mod	Ran	Sect	Shelf	Tray	Item
P	2	04	22	11	07	004







STRUCTURAL DEFECTS AND INSTABILITIES  
IN  
FREELY SUSPENDED LIQUID CRYSTAL FILMS

by

Jinzhong Pang

B.S., Nanjing University, China, 1982

M.S., Nanjing University, China, 1984

A thesis submitted to the  
Faculty of the Graduate School of the  
University of Colorado in partial fulfillment  
of the requirements for the degree of  
Doctor of Philosophy  
Department of Physics

1995



This thesis for the Doctor of Philosophy degree by

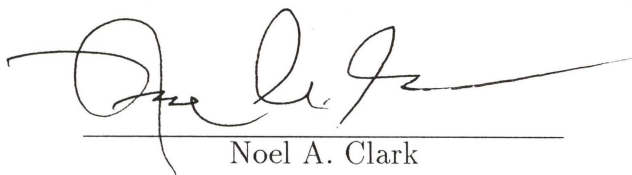
Jinzhong Pang

has been approved for the

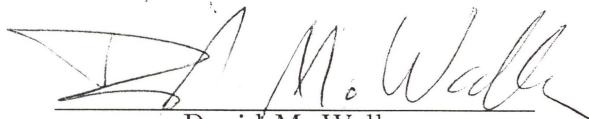
Department of

Physics

by



Noel A. Clark



David M. Walba

Date

11/22/95

Jinzhong, Pang (Ph.D., Physics)

Structural Defects and Instabilities in Freely Suspended Liquid Crystal Film

Thesis directed by Professor Noel A. Clark

Ultrathin freely suspended liquid crystal films (FSLCFs) are layered two-dimensional (2D) systems which are ideal for the study of 2D physics because of their rich phase and symmetry breaking behavior and almost exclusively internal interactions. We have studied structural defects and instabilities in tilted smectic FSLCFs of many different materials over a wide range of layer numbers. Our observations show that the range of possible phases, structural defects and instabilities in these films is considerably broader than previously realized. Here, we report our studies of string defects, twist-bend instabilities and splay instabilities in FSLCFs.

Until now, the defects identified in tilted smectic films are point topological defects of unit topological charge, in which the tilt orientation changes by  $\pm 2\pi$  upon traveling once around the defect point. We have discovered a variety of new defects in 2D tilted smectic systems (the "string" defects) in which there is discontinuity in tilt orientation along a line. We also find associated fractionally charged topological point defect structures. Our observations indicate the presence of additional stabilization mechanisms for 2D line defects and open the way for study of line defects in 2D systems.

Some of the most interesting structures in liquid crystals arise as a result of internal frustration. These are situations in which the local energetically ideal configuration cannot be extended to fill space, but must be accommodated by the appearance of defects, often in periodic arrays. We have discovered two new frustrated phases in FSLCFs: the twist-bend stripe phase and the splay



stripe phase. The twist-bend stripe phase is formed in an achiral compound with one aliphatic and one perfluoroalkyl chain and is a novel example of spontaneous chiral-symmetry breaking. This phase transition is mainly driven by the interior twist field generated by the steric interaction of molecules in non-polar films. The splay stripe phase, on the other hand, arises as a result of a polar ordering phase separation, and the instability of the ensuing domain boundaries.

## Acknowledgment

I greatly appreciate the help of many others in the completion of this thesis. First, I wish to express my heartfelt gratitude to my advisor, Professor Noel Clark, who introduced me to the fantastic world of two-dimensional physics. His insight into physics and his kind guidance and assistance to me were indispensable to the successful completion of this research. I also wish to express my sincere thanks to Professor David Walba from the Department of Chemistry for his insightful comments and timely assistance to me during this research.

In our wonderful research group, I am very grateful to Dr. Chris Muzny for helping me in countless ways, both in setting up the experiments and in analyzing the results. I owe a great deal to Dr. Matt Glaser, who not only offered many valuable suggestions for me to understand the experimental results but also spent his precious time proofreading this thesis. I also appreciate Darren Link for his proofreading the first draft of this thesis. Many thanks go to Dr. Joe MacLennan for sharing his valuable insights on this research with me, and to Art Klitnick for his frequent expert help with mechanics and electronics. During my studies, I benefited a great deal from our research group, for which special thanks go to Dr. Jiuzhi Xue, Dr. Aaron Rappaport, Dr. Zhong Zou, Dr. Rainer Malzbender, Dr. Dan Parks, Dr. Zhiming Zhuang, Dr. Qi Jiang, Renfan Shao and Cheol Park. I would also like to thank the staff of the Condensed Matter Laboratory office, Sally Hofmockel, Jen Buley, and Faleesha Hindman, for their kind help during my studies.

Outside our group, I greatly appreciate Dr. Jonathan V. Selinger of the Naval Research Laboratory and Dr. Lachezar Komitov of the Chalmers University of Technology in Sweden for sharing their valuable insights with me on this research.



I would like to thank my parents for their love and support throughout my life. I deeply cherish the memory of my mother, who firmly believed that knowledge is the only power and treasure in one's life. Because of her belief, she endured unbearable hardship to send her children to school. All my life-long achievements I owe to her. Finally, I want to give my heartfelt thanks to my wife, Xiaxian Zhang, for her love and support, and to my daughter, Lisa Pang, for the cheerful sunlight she has brought into our lives during our school life.

## Contents

I.	INTRODUCTION	1
1.1	Liquid crystal phase structures . . . . .	1
1.1.1	Nematic phase and order parameter . . . . .	1
1.1.2	Smectic phases . . . . .	2
1.2	Deformations in Liquid Crystals . . . . .	6
1.2.1	The splay, twist and bend deformations . . . . .	6
1.2.2	The helical structure . . . . .	6
1.2.3	Flexoelectric effect . . . . .	8
1.3	Liquid Crystal film and XY model . . . . .	10
1.3.1	Smectic films . . . . .	11
1.3.2	XY model . . . . .	14
1.3.3	Vortices and strings . . . . .	16
II.	Experimental Techniques	20
2.1	Oven and Liquid Crystal Film Fabrication . . . . .	20
2.2	Film layer number measurement . . . . .	21
2.2.1	Reflectivity of a film . . . . .	23
2.2.2	Experimental Set-up . . . . .	23
2.3	Visualization of Thin Tilted Smectic Liquid Crystal Films . . . . .	25
2.3.1	Experiment Set-up . . . . .	25
2.3.2	Mapping the molecular director field . . . . .	27
III.	STRING DEFECTS IN FSLCFs	35



	viii
3.1 Summary . . . . .	35
3.2 Introduction . . . . .	35
3.3 Observations of string . . . . .	36
3.4 The 2D XY models and strings . . . . .	43
 IV. A CHIRAL SYMMETRY BREAKING TWIST-BEND INSTABIL- ITY IN ACHIRAL FSLCFs	 47
4.1 Summary . . . . .	47
4.2 Introduction . . . . .	47
4.3 Experiment and Results . . . . .	48
4.4 Theory . . . . .	56
4.5 Discussion . . . . .	57
 V. A NOVEL SPLAY INSTABILITY IN FSLCFs	 60
5.1 Summary . . . . .	60
5.2 Introduction . . . . .	60
5.3 Polar symmetry breaking in FSLCFs . . . . .	62
5.4 Experiments and results . . . . .	68
 VI. CONCLUSIONS	 75

## List of Tables

2.1	Reflectivities of liquid crystal films . . . . .	26
6.1	Table: Comparison of twist-bend and splay instabilities. . . . .	76

## List of Figures

1.1	The arrangement of molecules in liquid crystal phases . . . . .	3
1.2	Frustrated smectic A phases . . . . .	4
1.3	Frustrated smectic C phases . . . . .	5
1.4	The splay, twist, and bend deformations in LC . . . . .	7
1.5	The arrangement of molecules in the cholesteric mesophase . . .	9
1.6	The steric interaction of dumb-bell-like molecules . . . . .	9
1.7	Meyer's model of curvature electricity . . . . .	10
1.8	The tilted smectic LC film geometry . . . . .	12
1.9	The C-vector and P-vector . . . . .	13
1.10	XY-model . . . . .	15
1.11	Director orientation $\phi$ along a polar line with an angle $\alpha$ . . . .	16
1.12	Molecular orientation in the neighborhood of a vertex . . . . .	18
2.1	Schematic diagram of the oven . . . . .	22
2.2	Schematic diagram of film thickness measurement set-up . . . .	24
2.3	Film holder and film geometry . . . . .	28
2.4	The DRLM images for different point vortices . . . . .	30
2.5	The DRLM images of vortices under uncrossed polarizers . . . .	31
2.6	The oblique light incidence of microscope in reflection model . .	32
2.7	The asymmetry of oblique light incidence to a tilted smectic film	33
2.8	A DRLM image and c-vector field of a -5 vortex . . . . .	34
3.1	The possible string's conformations . . . . .	37
3.2	Selected string's DRLM photos and c-vector fields . . . . .	39



	xi
3.3 A half-integer vortex-antivortex pair connected by a string . . .	44
3.4 Monto Carlo simulation of string defect . . . . .	44
3.5 Conformal mapping . . . . .	46
4.1 The twist and bend geometry in FSLCFs . . . . .	49
4.2 DRLM photomicrographs of CRL-EX-900084 freely suspended smectic C films. . . . .	51
4.3 DRLM photomicrographs of CRL-EX-900084 freely suspended smectic C films. . . . .	52
4.4 DRLM map of the twist-bend stripes . . . . .	54
4.5 Bilayer structures of films. . . . .	59
5.1 Polar ordered Freely suspended smectic-C film geometry . . . .	63
5.2 The splay stripe geometry . . . . .	65
5.3 The phase transition process of a polar multiple domain smectic- C film. . . . .	67
5.4 The chemical formula and the phase digram of DOBAMBC. . .	69
5.5 DRLM images of polar phase separation and splay stripe phase	70
5.6 DRLM image of a splay stripe and the underlying pattern of c-vector . . . . .	71
5.7 DRLM images of the splay instability . . . . .	72
5.8 The width of splay stripes vs temperature. . . . .	74

## CHAPTER I

### INTRODUCTION

Here, we report our studies of structural defects and instabilities in tilted smectic freely suspended liquid crystal films (FSLCFs). In this introduction, we briefly describe the structures of liquid crystals (LC), the relationship between symmetries and deformations, and the relationship between liquid crystal films and the XY model, which are closely related to our work.

#### 1.1 Liquid crystal phase structures

Besides the conventional states of matter, solid, liquid, and gas, liquid crystalline states occur in some strongly elongated molecules. In these states, the molecular mass centers are randomly positioned, or have no *positional order* in two or three spatial dimensions, but the molecules are more or less parallel to each other, or have *orientational order*. There are many different liquid crystal phases occurring in different liquid crystal materials at different temperatures. The structures of the liquid crystal phases are characterized by the arrangement of the molecules, the conformation of the molecules and the intermolecular interactions.

##### 1.1.1 Nematic phase and order parameter

The nematic phase is a state in which the molecules have orientational order, but the molecular centers of mass have no positional order in

three-dimensional (3D) space. The direction of average orientation of the long axes of the molecules is specified by a unit vector  $\mathbf{n}$ , called the director. The arrangement of molecules in the nematic phase is shown in Figure 1.1(b). The order parameter of a nematic phase can be defined as [1]

$$S = \left\langle \frac{3}{2} \cos^2 \theta - \frac{1}{2} \right\rangle, \quad (1.1)$$

where  $\theta$  is the polar angle between the long axis of the molecule and  $\mathbf{n}$ , and the angular brackets indicate a statistical average. It is clear that  $S$  goes to zero for an isotropic distribution of molecules such as that shown in Figure 1.1(a), and takes the value 1 when all the molecules are strictly parallel to each other. Typical values of  $S$  in the nematic phase are in the range 0.4 to 0.6.

### 1.1.2 Smectic phases

The smectic phases are states in which the molecules have orientational order and the molecular centers of mass have no positional order in two-dimensions thus comprising a layered phase. Smectic phases have a higher degree of position order than nematic phase. In the Smectic-A phases, the molecules are perpendicular to the layers ( Figure 1.1(c)), while in the Smectic-C phase, the molecules are tilted at an angle with respect to the layer normal(Figure 1.1(d)).

A number of frustrated Smectic phases have been discovered in strongly polar molecules[2]. For non-tilted phases, they are the monolayer ( $A_1$ ) phase, the bilayer ( $A_2$ ) phase and the partial bilayer ( $A_d$  and  $\tilde{A}$ ) phases shown in Figure 1.2. For tilted phases, they are the monolayer ( $C_1$ ) phase, the bilayer( $C_2$ ) phase and the partial bilayer( $C_d$  and  $\tilde{C}$ ) phases shown in Figure 1.3.



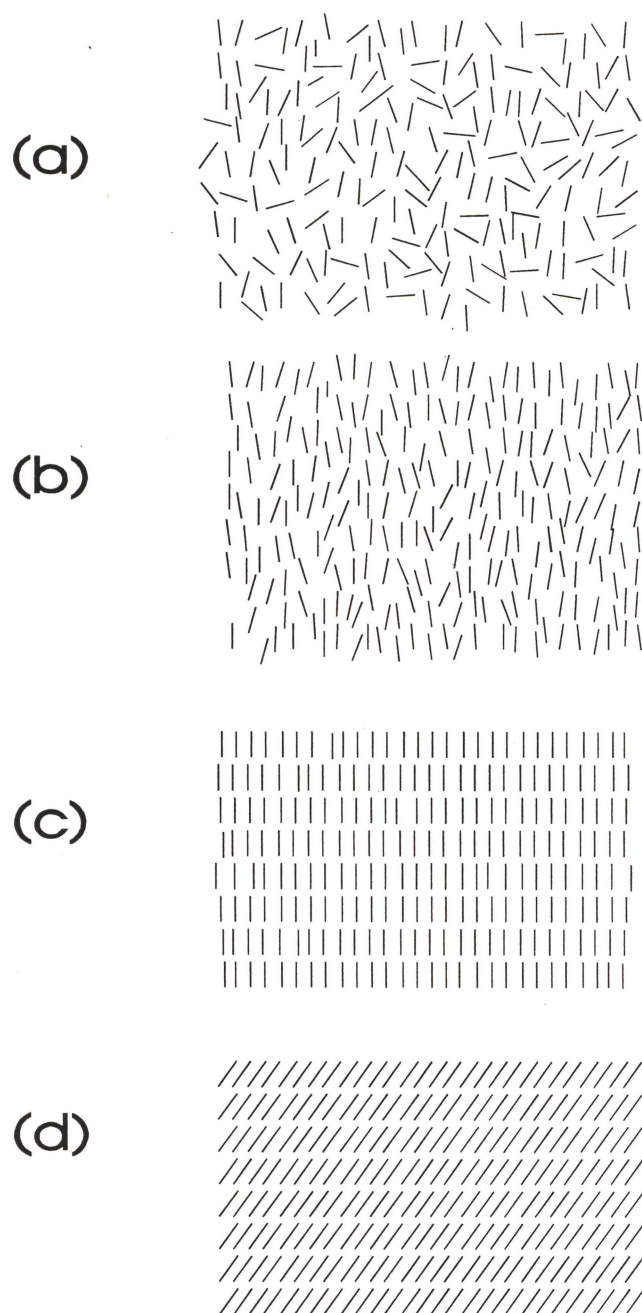


Figure 1.1: The arrangement of molecules in liquid crystal phases: (a) Isotropic, (b) Nematic, (c) Smectic A, and (d) Smectic C.

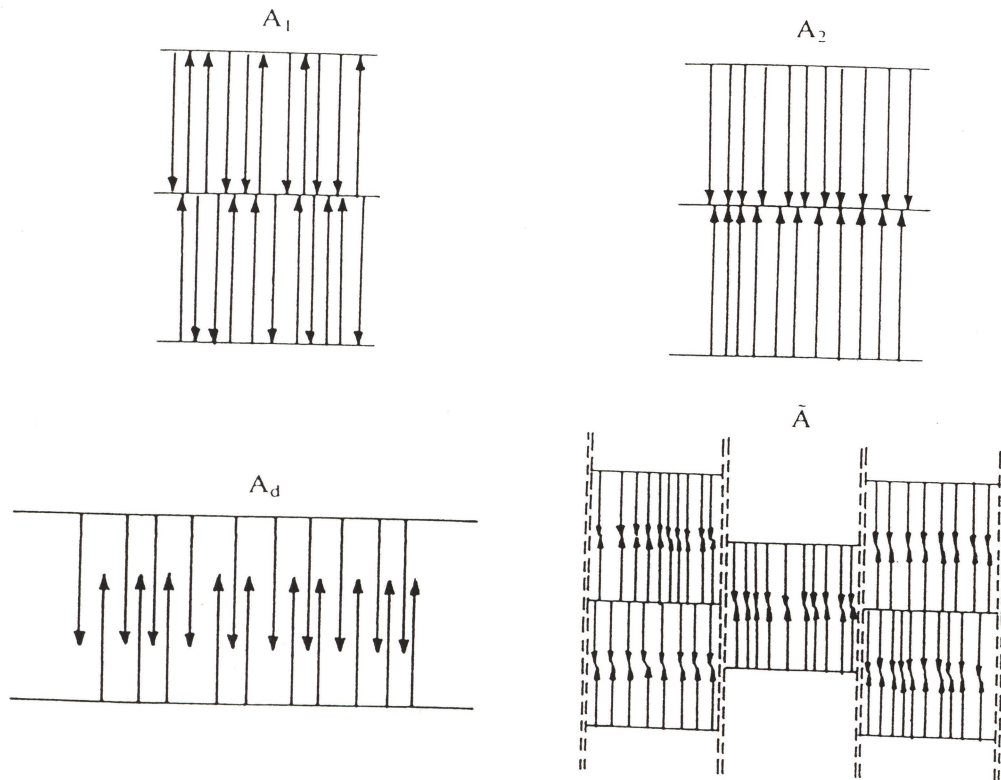


Figure 1.2: Frustrated smectic A phases

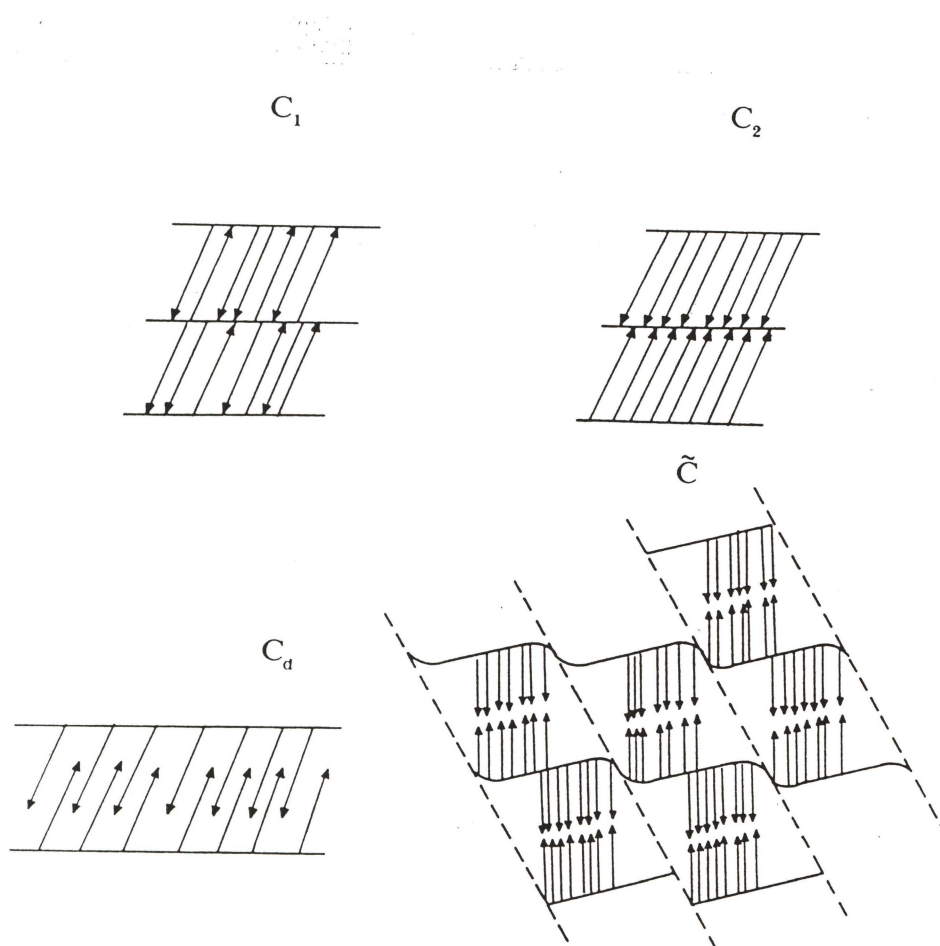


Figure 1.3: Frustrated smectic C phases

## 1.2 Deformations in Liquid Crystals

### 1.2.1 The splay, twist and bend deformations

An arbitrary deformation of a liquid crystal can be decomposed into a combination of three basic deformations, splay, twist and bend, which are shown in Figure 1.4. The Frank free energy of the nematic liquid crystal deformation is given by the equation

$$F = \frac{1}{2}[K_1(\nabla \cdot n)^2 + K_2(n \cdot \nabla \times n)^2 + K_3(n \times \nabla \times n)^2]. \quad (1.2)$$

Where,  $K_1$ ,  $K_2$ , and  $K_3$  are the splay, twist, and bend elastic constants respectively;  $\nabla \cdot n$ ,  $n \cdot \nabla \times n$ , and  $n \times \nabla \times n$  are the splay, twist, and bend of director  $n$  respectively.

There can exist a uniform twist structure, or helical structure, in liquid crystals. But there is no continuous structure that can contain uniform splay or bend. If there is an intrinsic polarity in the molecular ordering of a liquid crystal, then that liquid crystal would have a fine domain structure accommodated by the appearance of defects. We report a novel splay stripe phase in FSLCFs in Chapter V.

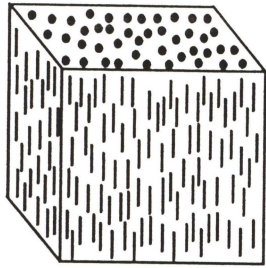
### 1.2.2 The helical structure

If molecules in a nematic are chiral, or the molecules are different from their mirror images, the structure undergoes a helical deformation as shown in Figure 1.5. In such a chiral system, the Frank free energy can be written as

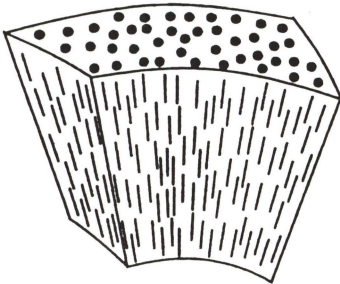
$$F = \frac{1}{2}[K_1(\nabla \cdot n)^2 + K_2(n \cdot \nabla \times n - q)^2 + K_3(n \times \nabla \times n)^2]. \quad (1.3)$$

Where  $q$  is the equilibrium twist of a chiral system.

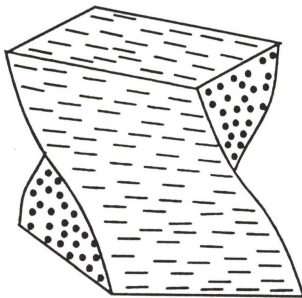




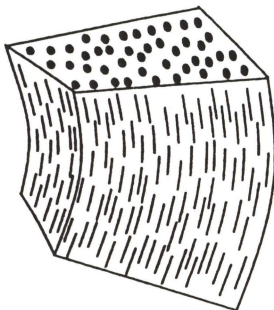
no deformation



splay



twist



bend

Figure 1.4: The splay, twist, and bend deformations in LC

If we call the  $z$ -axis the helical axis, we have the following structure for  $\mathbf{n}$

$$\begin{cases} n_x = \cos(q_0 z + \phi) \\ n_y = \sin(q_0 z + \phi) \\ n_z = 0 \end{cases} \quad (1.4)$$

Both the helical axis ( $z$ ) and the value  $\phi$  are arbitrary. For a racemic mixture of right- and left-hand molecules, the system has no helical deformation.

For an achiral system, under certain conditions, molecules would tend to form a local twist deformation without a preference of the sign of twist [1]. Figure 1.6 shows two twist deformations for dumb-bell-like molecules due to the steric interaction. In this system, the free energy has two minima for the twist and the twist has a large fluctuation and varies in space. The Frank free energy can be written as:

$$F = \int d^2r \left[ \frac{1}{2} K_1 (\nabla \cdot \mathbf{n})^2 + \frac{1}{2} K_2 (\mathbf{n} \cdot \nabla \times \mathbf{n} - q)^2 + \frac{1}{2} K_3 (\mathbf{n} \times \nabla \times \mathbf{n})^2 + \frac{1}{2} \kappa (\nabla q)^2 + \frac{1}{2} t q^2 + \frac{1}{4} m q^4 \right]. \quad (1.5)$$

The second term is a Landau free energy which generates the appearance of  $q$ . At the present stage no helices of this kind have been found in bulk liquid crystals. In Chapter IV, we report our first observation of a short range helical order or a chiral-symmetry-breaking twist-bend instability in achiral FSLCFs.

### 1.2.3 Flexoelectric effect

If there is an intrinsic polarity in the molecular ordering of a liquid crystal, then that liquid crystal in its lowest energy structure will tend to be splayed and ferroelectric [5]. Figure 1.7(a) shows an unstrained nematic structure containing polar molecules. Figure 1.7(b) shows a splay structure in

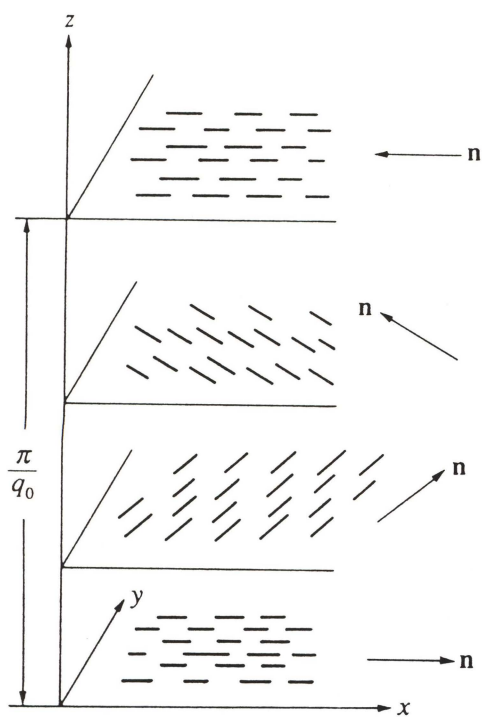


Figure 1.5: The arrangement of molecules in the cholesteric mesophase.

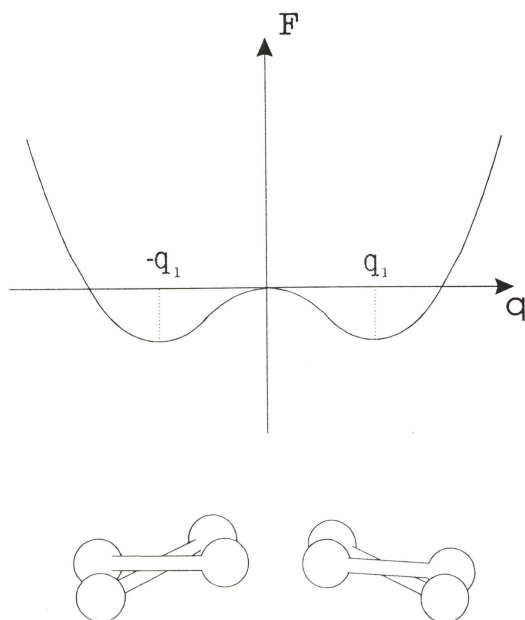


Figure 1.6: The steric interaction of dumb-bell-like molecules.

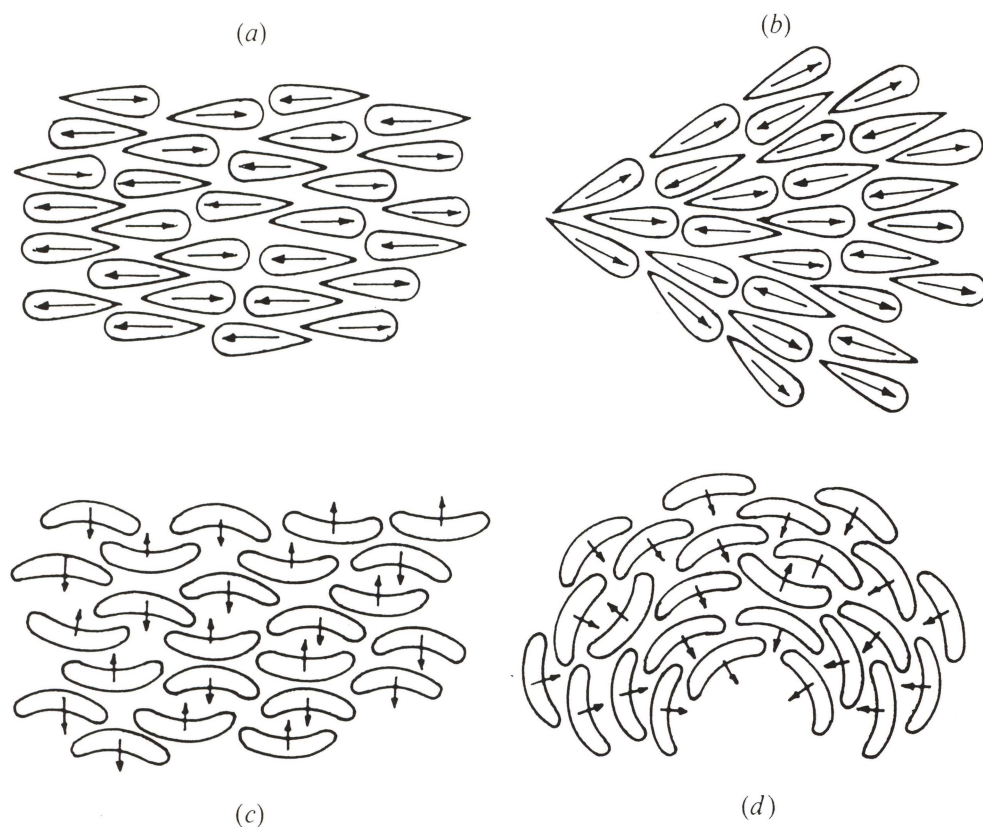


Figure 1.7: Meyer's model of curvature electricity

which splay and polarization are coupled by the wedge shape of the molecule. The splay structure can be induced by an electric field, cell boundary, or the film's surfaces. Figure 1.7(c) shows an unstrained nematic structure containing banana-shaped molecules. Figure 1.7(d) shows a bend structure in which bend and polarization are coupled.

### 1.3 Liquid Crystal film and XY model



### 1.3.1 Smectic films

Freely suspended liquid crystal films are layered two-dimensional systems which are stabilized by their own layer structure. As early as 1922, Freidel[4] described FSLCFs in his classic treatise on liquid crystals. In 1973, Meyer and Clark[13] started to study textures in FSLCFs. Now, FSLCFs play an important role in the study of liquid crystal structure and 2D physics because of their rich phase and symmetry breaking behavior, and almost exclusively internal interactions.

Films can be drawn over a hole in a glass microscope cover slip. It is possible to draw films of almost any desired thickness from 2 layers to on the order of thousands of layers. We have successfully drawn one layer films with a liquid crystal material from 3M (CRL-EX-900084). The film geometries are shown in Figure 1.8. We have studied three kinds of film layer structures: normal smectic C films, bilayer films, and polar films. They represent different types of symmetry. The local mean molecular long axis, given by the director  $\mathbf{n}$ , is tilted relative to the layer and film plane normal through an equilibrium angle  $\theta$ . The projection of  $\mathbf{n}(x, y)$  onto the film plane defines a 2D “c director” unit vector field  $\mathbf{c}(x, y)$  having a local mean scalar azimuthal orientation field  $\phi(x, y)$  which can be visualized using depolarized reflected light microscopy(DRLM). In Figure 1.9, The “Tees” represent c-vectors, and the small bars indicate the ends of the molecules closest to the surface. In a polar smectic film, for the same c-vectors, the underling polar molecule can be oriented in either direction. In order to distinguish these two cases, we introduce a P-vector, indicated by the arrow, which is a simple projection of the vector  $n$  onto the layer plane. There are two possible configurations of a polar tilted film as regards the combination of c-vector and p-vector: c-vectors are parallel to p-vectors or c-vectors are anti-parallel to the p-vectors(Figure 1.9).

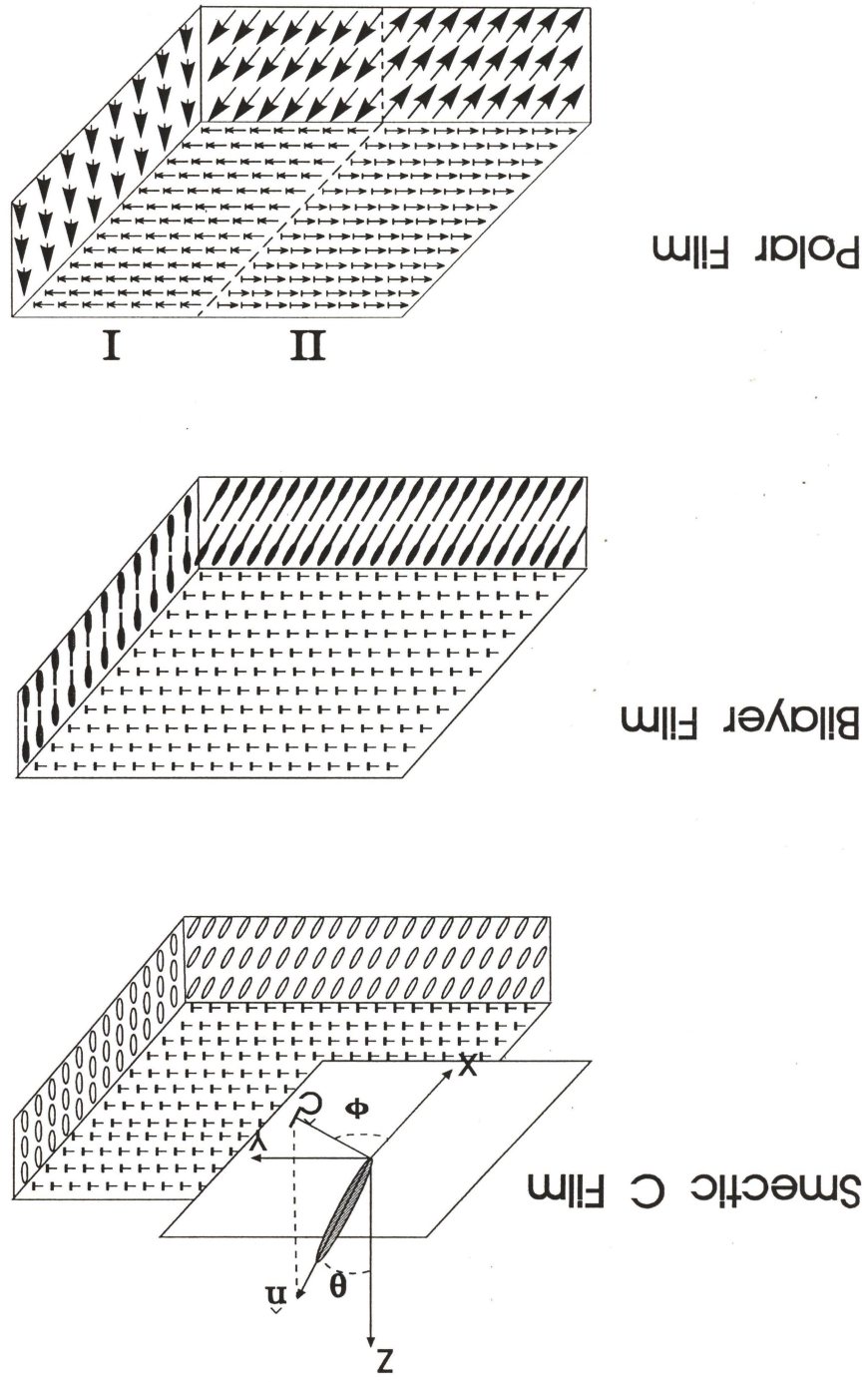


Figure 1.8: The tilted smectic LC film geometry.

## C-Vector and P-Vector For Strongly Polar Liquid Crystal Films

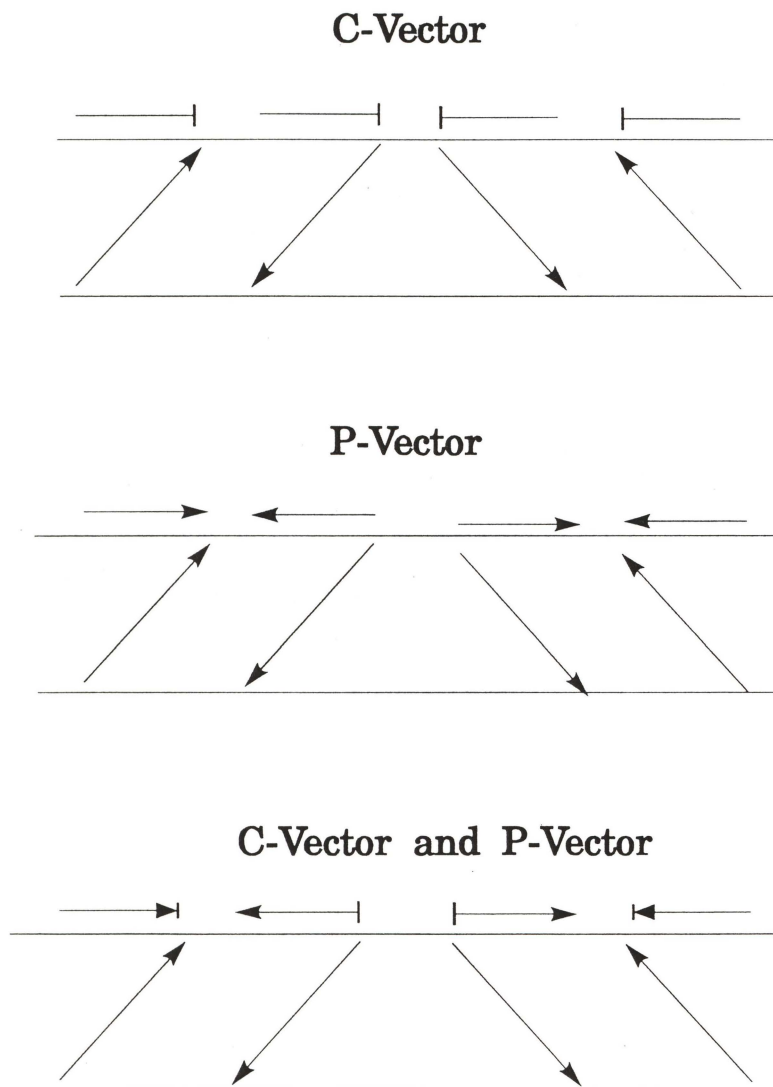


Figure 1.9: The C-vector and P-vector in tilted smectic LC films.

The Frank free energy of FSLCFs is given by the equation [9]

$$F = \frac{1}{2}[K_s(\nabla \cdot c)^2 + K_b(\nabla \times c)^2]. \quad (1.6)$$

Here,  $\nabla = \hat{i}\partial/\partial x + \hat{j}\partial/\partial y$ .  $K_s$  and  $K_b$  are the 2D splay and bend elastic constants, which have the following relation to the bulk elastic constants  $K_1$  (splay),  $K_2$  (twist), and  $K_3$  (bend):

$$\begin{cases} K_s = hK_1 \sin^2 \theta, \\ K_b = h[K_2 \sin^2 \theta \cos^2 \theta + K_3 \sin^4 \theta]. \end{cases} \quad (1.7)$$

In most cases,  $\theta$  is about  $20^\circ$ , so  $\sin^4 \theta \ll \sin^2 \theta$  and the bend elastic constant  $K_b$  is mainly contributed by  $K_2$ . So, in an LC film, the bend elastic constant  $K_b$  is smaller than the splay elastic constant  $K_s$ . In contrast, for bulk LC, the bend elastic constant  $K_3$  is larger than the splay elastic constant  $K_1$ .

In many cases, the full form of Equation 1.6 is too complex to be of practical use. With a further approximation, assuming  $K_b = K_s = K$  and writing  $c = \cos(\phi)\hat{i} + \sin(\phi)\hat{j}$ , the free energy can be simplified to

$$F = \frac{K}{2}(\nabla\phi)^2. \quad (1.8)$$

### 1.3.2 XY model

The 2D XY-model deals with two-component classical spins ( $S_x, S_y$ ) normalized to unit length  $S_x^2 + S_y^2 = 1$ , on a 2D square lattice, and interacting with their nearest neighbors (Figure 1.10). After some transformations, this model also describes a classical Coulomb gas, a fluctuating surface, or a superfluid film. The Hamiltonian of this model can be written as

$$H = -K \sum_{\langle i,j \rangle} S_i \cdot S_j = -K \sum_{\langle i,j \rangle} \cos(\theta_i - \theta_j). \quad (1.9)$$

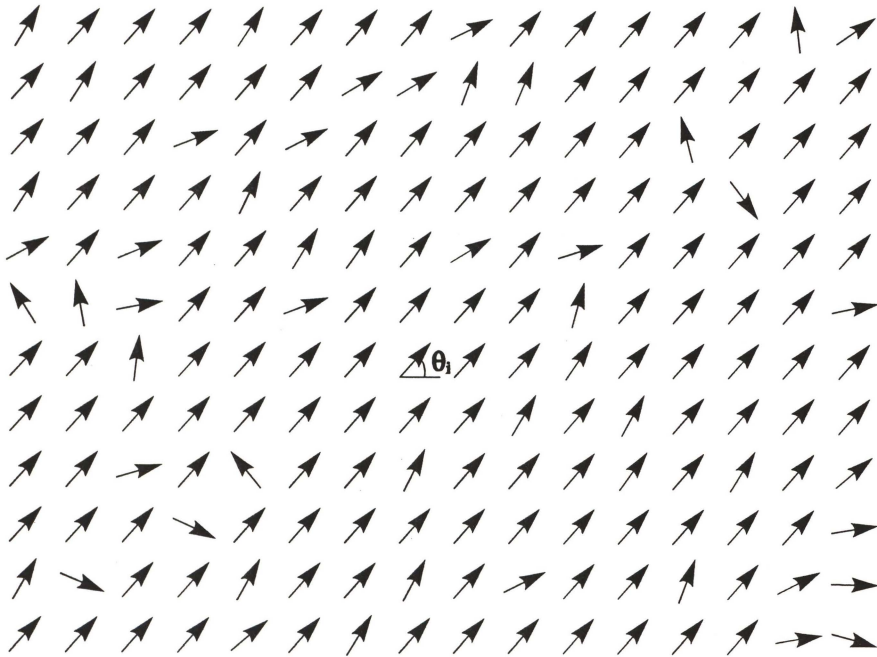


Figure 1.10: XY-model



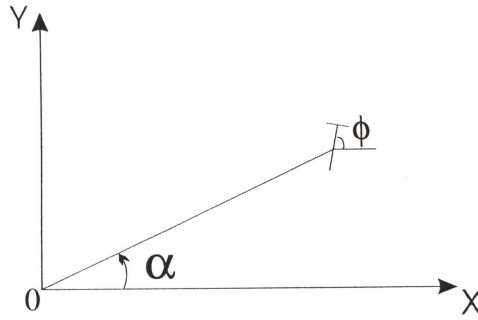


Figure 1.11: Director orientation  $\phi$  along a polar line with an angle  $\alpha$ .

At low enough temperature, the energetic term favors the alignment of spins, and we can expand  $\cos(\theta_i - \theta_j)$  near  $\theta_i - \theta_j = 0$ . And at sufficiently large scale with respect to the lattice spacing, the microscopic structure of the lattice can be neglected. Under these conditions, the Hamiltonian can be written as

$$H = \frac{K}{2}(\nabla\theta)^2. \quad (1.10)$$

Comparing this Hamiltonian with the free energy of the film, we see that they have the same form. So, a tilted smectic FSLCF is a physical 2D system which can be used to test the XY-model.

### 1.3.3 Vortices and strings

From the free energy Equation 1.8 of the film and the Hamiltonian 1.10 of the XY-model, the classical field equation is

$$\Delta\phi = 0. \quad (1.11)$$

For which a simple and important vortex solution is

$$\phi = s\alpha + c. \quad (1.12)$$

Where  $\alpha$  is the polar angle in cylindrical coordinates (Figure 1.11) and  $c$  is a constant. The topological charge, denoted  $s$ , is the strength of the vortex and

has integer values for polar systems and half-integer values for apolar systems. Figure 1.12 shows some examples of vortices with different topological charges and values for  $c$ .

A system with many vortices is hard to describe by equations like 1.12, but can be easily described by a harmonic function in the 2D complex plane. In the complex plane with  $z = x + iy$ , we can describe a +1 vortex at  $z_0$  as  $S_x + iS_y = e^{i\phi} = \exp(i \text{Arg}[(z - z_0)])$ . The function  $\phi(x, y)$  is harmonic everywhere except at the point  $z_0$ . For a system with  $n$  vortices with topological charges  $q_j, (j = 1, n)$  and at positions  $z_j, (j = 1, n)$  respectively, the harmonic function  $\phi(x, y)$  can be written

$$\phi = \text{Arg}\left[\prod_{j=1}^n (z - z_j)^{q_j}\right] + \phi_\infty. \quad (1.13)$$

We introduce the following harmonic function to simplify calculations.

$$G(z) = \rho e^{i\phi} = e^{i\phi_\infty} \prod_{j=1}^n (z - z_j)^{q_j}. \quad (1.14)$$

For harmonic functions, we have the Cauchy-Riemann equation,

$$(\nabla\phi)^2 = (\nabla \ln \rho)^2 = \nabla \cdot (\ln \rho \nabla \ln \rho). \quad (1.15)$$

The free energy can be evaluated for sufficiently small  $r_0$ . If  $C_j$  is the circle surrounding  $z_j$ ,

$$\begin{aligned} F &= K/2 \int d^2x (\nabla\phi)^2 \\ &= -K/2 \sum_j \oint_{C_j} ds \ln \rho n \cdot \nabla \ln \rho \\ &= -2\pi K \sum_{(i,j)} q_i q_j \ln |z_i - z_j| + \sum_i q_i^2 \pi \ln(1/r_0). \end{aligned} \quad (1.16)$$

For a  $\pm 1$  vortex pair, at distance  $r_{12}$ , the interaction energy is  $2\pi K \ln(r_{12}/r_0)$ . If the system's temperature is higher than  $T_c$ , where  $T_c = \pi K/2k_B$ , the creation of well-separated vortices is favored and disorder increases. Young et al.[9]

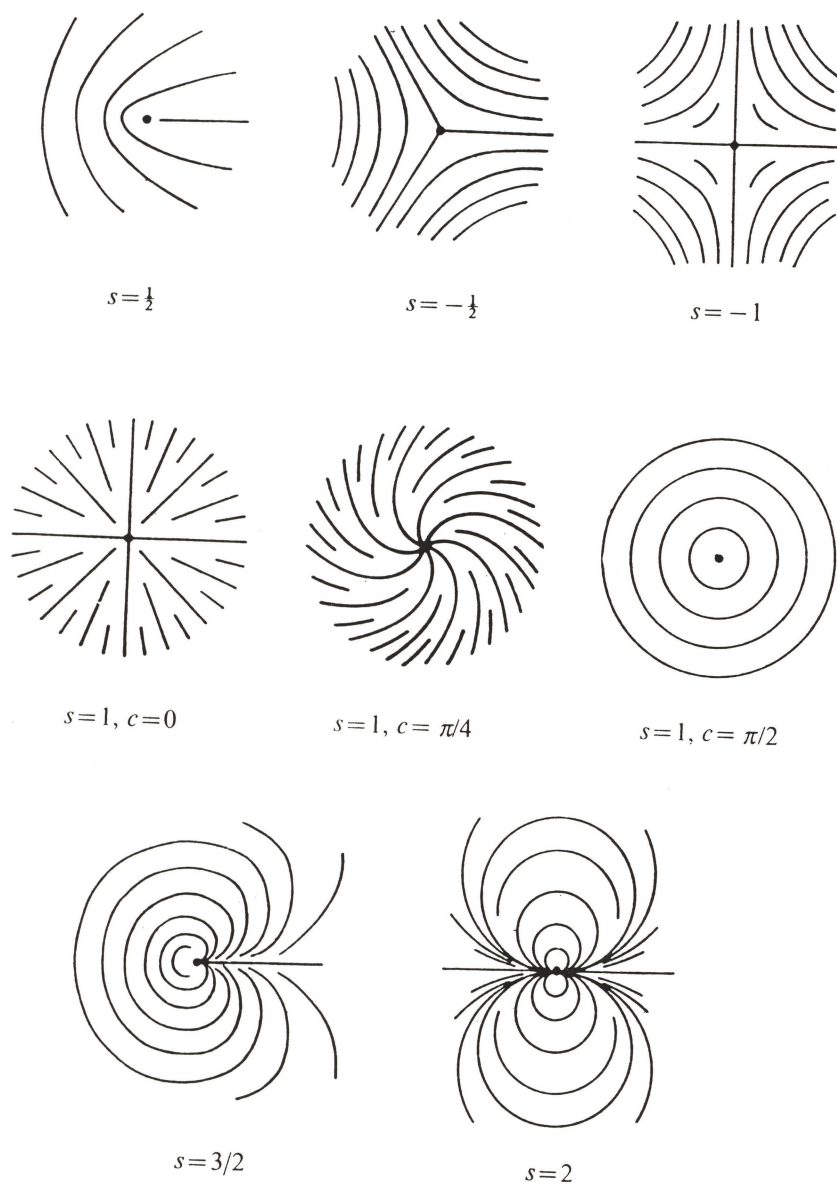


Figure 1.12: Molecular orientation in the neighbourhood of a vertex.

performed a light-scattering study of tilted smectic FSLCFs and observed this transition that was predicted by Kosterlitz and Thouless[3].

Let us consider the conformation of a simple vortex.  $G(z) = \sqrt{z}$  represents a  $+1/2$  vortex in an apolar system that has been observed in nematic liquid crystals. It has a line defect at which directors are antiparallel in a polar system. This line defect has not been observed in the past in the smectic C phases. In Chapter III, we report our first observation of line defects in tilted smectic FSLCFs [29]. Our observations indicate the presence of additional stabilization mechanisms for 2D line defects and open the way for the study of line defects in the 2D XY-model.

## CHAPTER II

### Experimental Techniques

#### 2.1 Oven and Liquid Crystal Film Fabrication

It is a technical challenge to design an oven that has all of the following requirements: It can fabricate uniform freely suspended liquid crystal films with thickness down to  $30\text{\AA}$  and keep films stable in the environment. The temperature of the oven must be uniform and precisely controllable. The oven must facilitate measurement of film characteristics. It must be compact enough to fit in a microscope stage. It must be easily manipulated.

Through many years of experience we have developed an oven which successfully meets all of these design requirements. This oven is shown in Figure ???. This oven basically includes two parts: The sample chamber (block 7) and bottom (block 8). Minco heaters and a thermistor are sandwiched between these two blocks. The temperature is controlled by an INSTTECH temperature controller installed in a IBM PC and a temperature stability of  $0.01\text{K}$  is achieved. The tilted windows improve the image contrast critical for a microscope operating in the reflection mode. A  $3\text{mm} \times 10\text{mm}$  hole in a glass cover slip which is glued to the sample holder is used for drawing films. Films are reliably made under continuous observation by utilizing a movable holder, a movable and rotatable spade which is mounted on a stainless steel rod, and a Newport linear motor with controllable speed. The small piece of black glass located very close to the sample is used to calibrate the 4% optical reflectivity.



The entire oven is thermally insulated with Balsa wood and mounted on a rotatable XY microscope stage.

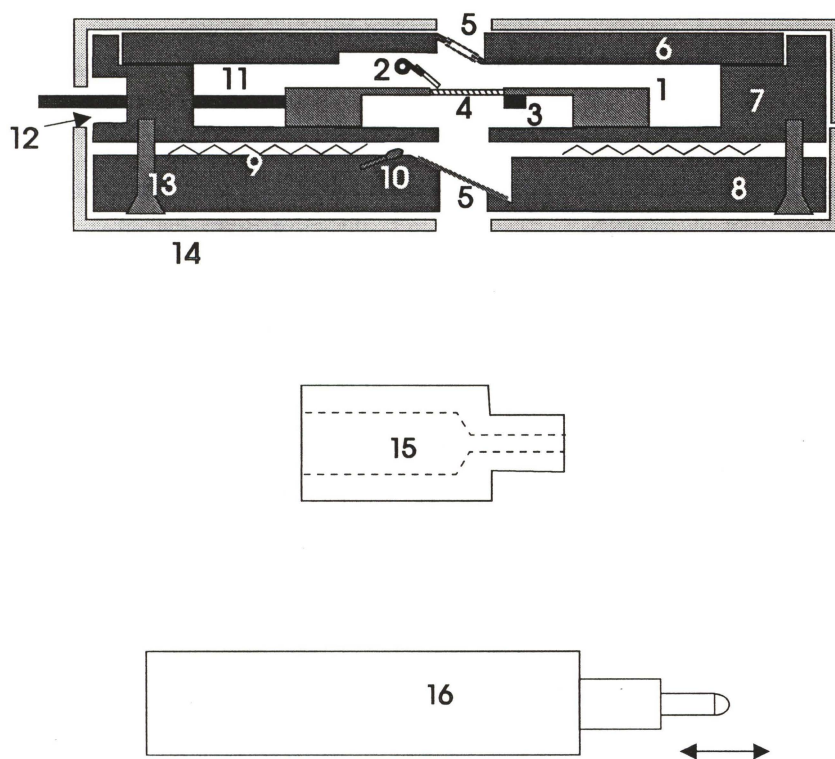
To fabricate a film, the following procedure is followed:

1. Place sample of liquid crystal material next to the opening in the glass cover slip on the end of cover slip opposite the push rod.
2. Heat the oven to the designed temperature, which depends on the liquid crystal material being used.
3. Adjust the positions of spreader and sample holder until the spreader touches the end of the sample hole.
4. Adjust the XY stage to bring the spreader into the microscope's field of view.
5. Mount the motorizer adapter to the oven and insert the linear motorizer into the adapter.
6. Apply a small torque on the spreader.
7. Start the linear motorizer and watch the newly fabricated film with microscope.

Several tries may be necessary to get a satisfactory film.

## **2.2 Film layer number measurement**

Almost all physical properties of thin films depend on their layer number. For some films with odd-even effects, we need to know the exact number of layers. So, it is very important to measure the exact layer number of films.



- |                          |                                |
|--------------------------|--------------------------------|
| 1. Sample Holder         | 9. Minco Heaters               |
| 2. Spreader              | 10. Thermistor                 |
| 3. Black Glass           | 11. Pushing Rod                |
| 4. LC Film               | 12. Motorizer Adaptor Notch    |
| 5. Double Tilted Windows | 13. Screws                     |
| 6. Oven Cover            | 14. Balsa Wood Heat Insulators |
| 7. Oven Sample Block     | 15. Linear Motorizer Adaptor   |
| 8. Oven Bottom Block     | 16. Newport Linear Motorizer   |

Figure 2.1: The oven for the LC film fabrications and measurements.

### 2.2.1 Reflectivity of a film

The thickness of a film may be difficult to measure and may change as a function of temperature, but the layer number of a film can be measured by measuring the reflectivity of the film. The reflectivity of a film is very sensitive to the film thickness which changes by about  $30\text{\AA}$  for each incremental change in layer number. So, the reflectivity changes significantly as a function of the layer number of the film.

A uniform thin smectic film is a uniaxial dielectric film whose optic axis is parallel to the director. Due to large fluctuations in the molecular directors in a film, the local optic axis is not fixed. If we use randomly polarized light to measure the reflectivity, the film can be treated as a homogeneous dielectric film with an average index of refraction  $n = 1.5$ . For a film of thickness  $h$ , the reflectivity  $R$  for normal incidence light of wave length  $\lambda$  is given by[8]

$$R = \frac{2r^2(1 - \cos 2\beta)}{1 - 2r^2 \cos 2\beta + r^4}, \quad (2.1)$$

where

$$\beta = \frac{2\pi}{\lambda}nh,$$

and

$$r = \frac{1 - n}{1 + n}.$$

### 2.2.2 Experimental Set-up

A schematic diagram of the thin film reflectivity experiment set-up is shown in Figure 2.2. A randomly polarized HeNe laser is used as a light source of wave length  $6328\text{\AA}$ . A 50% beamsplitter transmits the source laser beam and reflects the reflected laser beam from the thin film to the photodiode. A lens beneath the oven focuses the laser beam onto the film inside the oven. The reflected beams from the tilted oven windows are deflected out of the beam

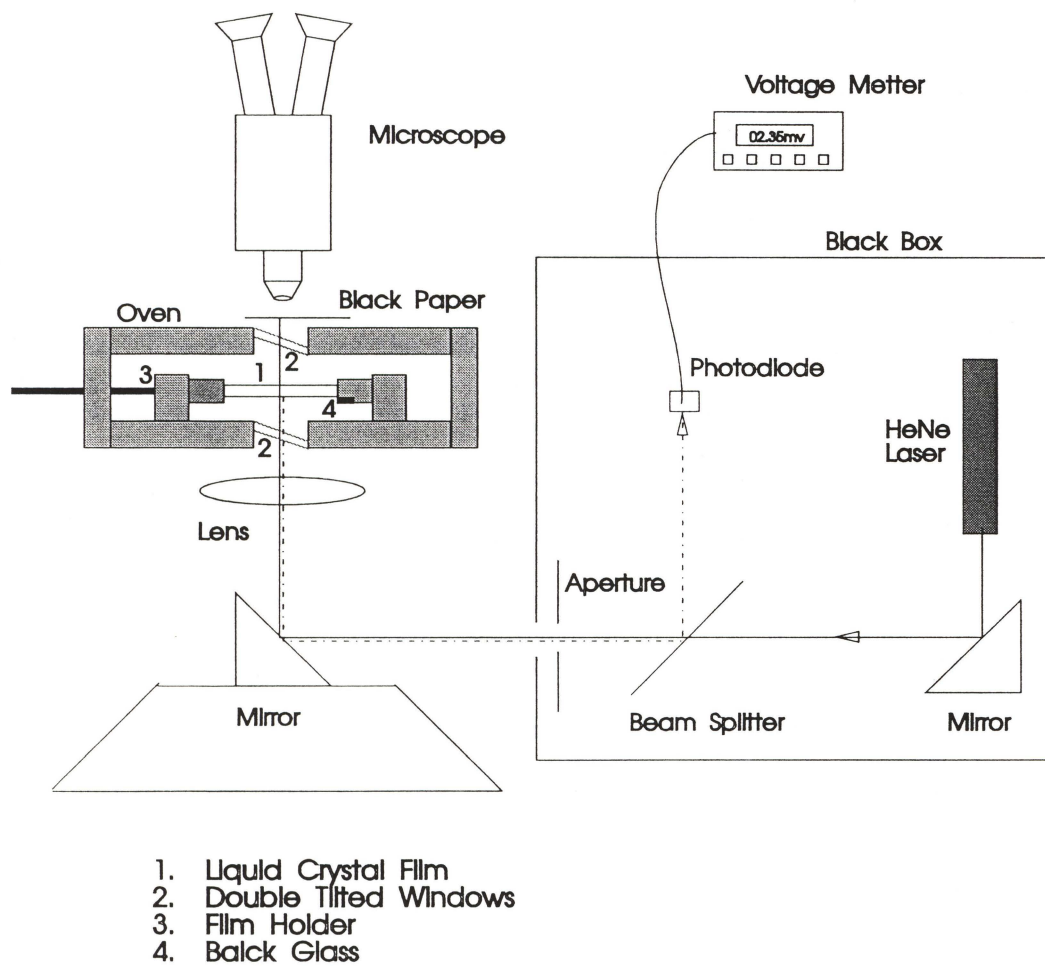


Figure 2.2: Schematic diagram of film thickness measurement set-up

path and do not interfere with the reflected beam incident on the photodiode. A piece of black paper blocks any reflective sources and light sources outside of the oven. The reflected beams from the surfaces of the lens diverge and are blocked by the aperture. Adjustable mirrors are used to adjust the laser beams so that the reflected beam retraces exactly the path of the incident beam. A small piece of black glass is attached to the film holder and can be moved to the focal point of the laser beam to measure the 4% reflectivity from the front surface. Then, the measurements of the film's reflectivity are compared against the measurement of this black glass to obtain the absolute reflectivity of the film. The intensity of the reflected laser beam is measured by a photodiode. For example, suppose the readout of photodiode voltage of black glass is 6.0 mv, Then, a table can be made such as Table 2.1 from which one can instantly tell the layer number of a film from the photodiode voltages. This table works well in most cases since a typical layer thickness is about  $30\text{\AA}$  and the average index of refraction is about 1.5 for liquid crystals. On the other hand, the index of refraction and layer thickness can be determined by measuring the reflectivity of films of several different layer numbers and then fitting the data to reflectivity formula.

## **2.3 Visualization of Thin Tilted Smectic Liquid Crystal Films**

### **2.3.1 Experiment Set-up**

Due to the weak optical properties of ultrathin liquid crystal films, the visualization of such films needs special microscopy and an intense light source. Figure 2.3(a) shows the schematic for depolarized reflected light microscopy used in our experiments. The microscope was used was a Zeiss ULTRAPHOT



**Table 2.1: Reflectivities of Liquid Crystal Films**  
 ( $n_{ave} = 1.5, \lambda = 6328\text{\AA}, V_{\text{Black Glass}} = 6.0\text{mv}$ )

Layer #	Thickness( $\text{\AA}$ )	Reflectivity	mv
1	30	0.0003	0.052
2	60	0.0014	0.207
3	90	0.0031	0.464
4	120	0.0055	0.819
5	150	0.0084	1.267
6	180	0.0120	1.805
7	210	0.0162	2.426
8	240	0.0208	3.122
9	270	0.0259	3.886
10	300	0.0314	4.709
11	330	0.0372	5.584
12	360	0.0433	6.502
13	390	0.0497	7.452
14	420	0.0562	8.427
15	450	0.0628	9.417
16	480	0.0694	10.414
17	510	0.0761	11.410
18	540	0.0826	12.395
19	570	0.0891	13.364
20	600	0.0954	14.308
21	630	0.1015	15.222
22	660	0.1073	16.098
23	690	0.1129	16.932
24	720	0.1181	17.717
25	750	0.1230	18.450
26	780	0.1275	19.126
27	810	0.1316	19.742
28	840	0.1353	20.294
29	870	0.1385	20.779
30	900	0.1413	21.196
31	930	0.1436	21.542
32	960	0.1454	21.815
33	990	0.1468	22.014
34	1020	0.1476	22.139
35	1050	0.1479	22.188
36	1080	0.1477	22.162
37	1110	0.1471	22.061
38	1140	0.1459	21.885
39	1170	0.1442	21.635
40	1200	0.1421	21.311

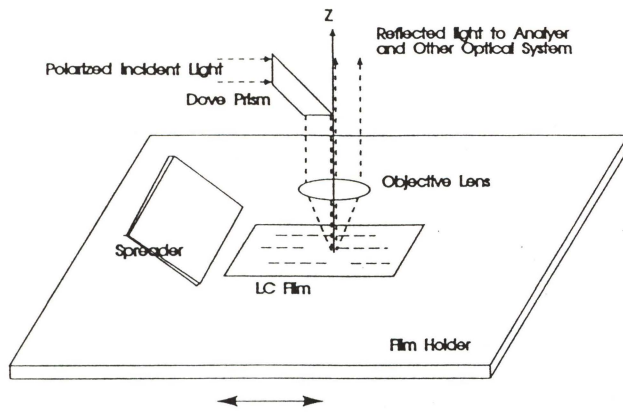
with a modified light source which can be switched between a 200W high-pressure mercury lamp and a laser. In order to get maximum contrast, all windows in the film oven in the light path are tilted and a dove prism is used to reflect the light source to the film instead of the beam splitter inside the Zeiss ULTRAPHOT microscope.

### 2.3.2 Mapping the molecular director field

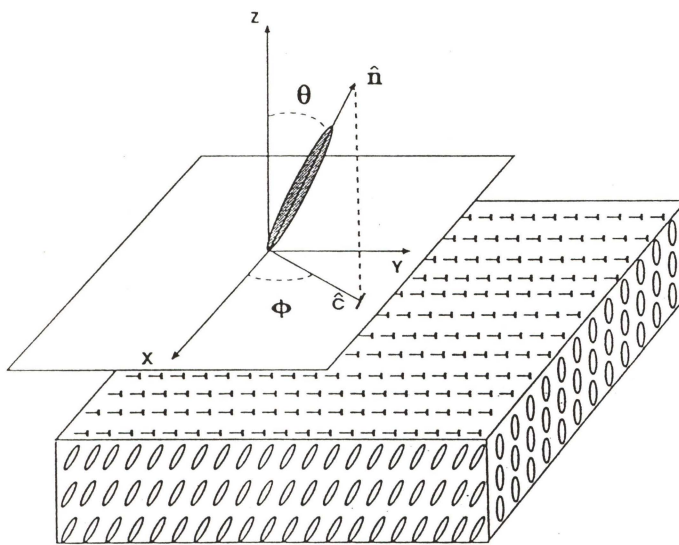
In the experiment, the polarized light illuminates the film with nearly normal incident light and the reflected light is imaged through an analyzer [figure 2.3(a)]. The film geometry is shown in Figure 2.3(b). The local mean molecular long axis, given by the director  $\mathbf{n}$ , is tilted relative to the layer and film plane normal through an equilibrium angle  $\theta$ . The projection of the director  $\mathbf{n}(x, y)$  onto the film plane defines a 2D “c-director” unit vector field  $\mathbf{c}(x, y)$  having a local mean scalar azimuthal orientation  $\phi(x, y)$  which can be visualized using depolarized reflected light microscopy (DRLM). Due to the optically anisotropic properties of liquid crystals, the index of refraction for polarized incident light depends on the relative angle between the polarization vector and the local liquid crystal molecular orientation. The polarization vector of the reflected light rotates toward the local liquid crystal molecular orientation. In the limit that the film thickness  $h \ll \lambda_0$ , the reflection coefficient,  $R(\phi)$ , after the crossed analyzers is given by [10]

$$R(\phi) \cong [2\pi(h/\lambda_0)(n_{\parallel}^2 - n_{\perp}^2) \sin(2\phi)]^2, \quad (2.2)$$

Where  $n_{\parallel}$  and  $n_{\perp}$  are refractive indices parallel to and perpendicular to  $\mathbf{n}$  and  $\phi$  is the angle between polarization vector of incident light and local liquid crystal molecular orientation. Figure 2.4 shows the DRLM images for different point vortices and the images for unit vortices are identical. These DRLM



(a)



(b)

Figure 2.3: (a) Schematic of film holder and optical arrangement.  
 (b) Freely suspended tilted smectic film geometry.

images show that  $R(\phi)$  has fourfold degeneracy. Upon rotation of the sample, the images for +1 vortices do not change, but the images for -1 vortices rotate with twice the speed in the same direction as the sample. By this method, we still cannot distinguish the bend vortex and the splay vortex. By slightly uncrossing the analyzers, the four dark brushes for a unit vortex merge into two dark brushes [Figure 2.5] and now the two dark brushes are oriented in different directions for bend and splay vortices. For example, if the vertical polarizer is rotated a few degrees clockwise, then, if the molecules point between  $0^\circ$  to  $90^\circ$  or  $180^\circ$  to  $270^\circ$  with respect to horizontal polarizer, they get brighter, otherwise, if the molecules point between  $90^\circ$  to  $180^\circ$  or  $270^\circ$  to  $360^\circ$  with respect to horizontal polarizer, they get dimmer. For a tilted liquid crystal film, this remaining twofold degeneracy can be removed by carefully studying the DRLM image in our system with obliquely incident light [figure 2.6]. If both the polarization vector and liquid crystal molecules in a area lie in the plane of incident and if they are tilted in the same direction as shown in Figure 2.7(a), the incident light senses a larger index of reflection for the film and the DRLM image has high contrast in that area. On the otherhand, if the polarization vector and liquid molecules are tilted in different directions as shown in Figure 2.7(b), then the incident light senses a smaller index of reflection for the film and the DRLM image has low contrast in that area. Hence, the optical reflectivity is sufficient to uniquely map the molecular orientation field for liquid crystal films. Figure 2.8 shows a DRLM image of a -5 vortex under crossed polarizers in our system and its c-vector field.



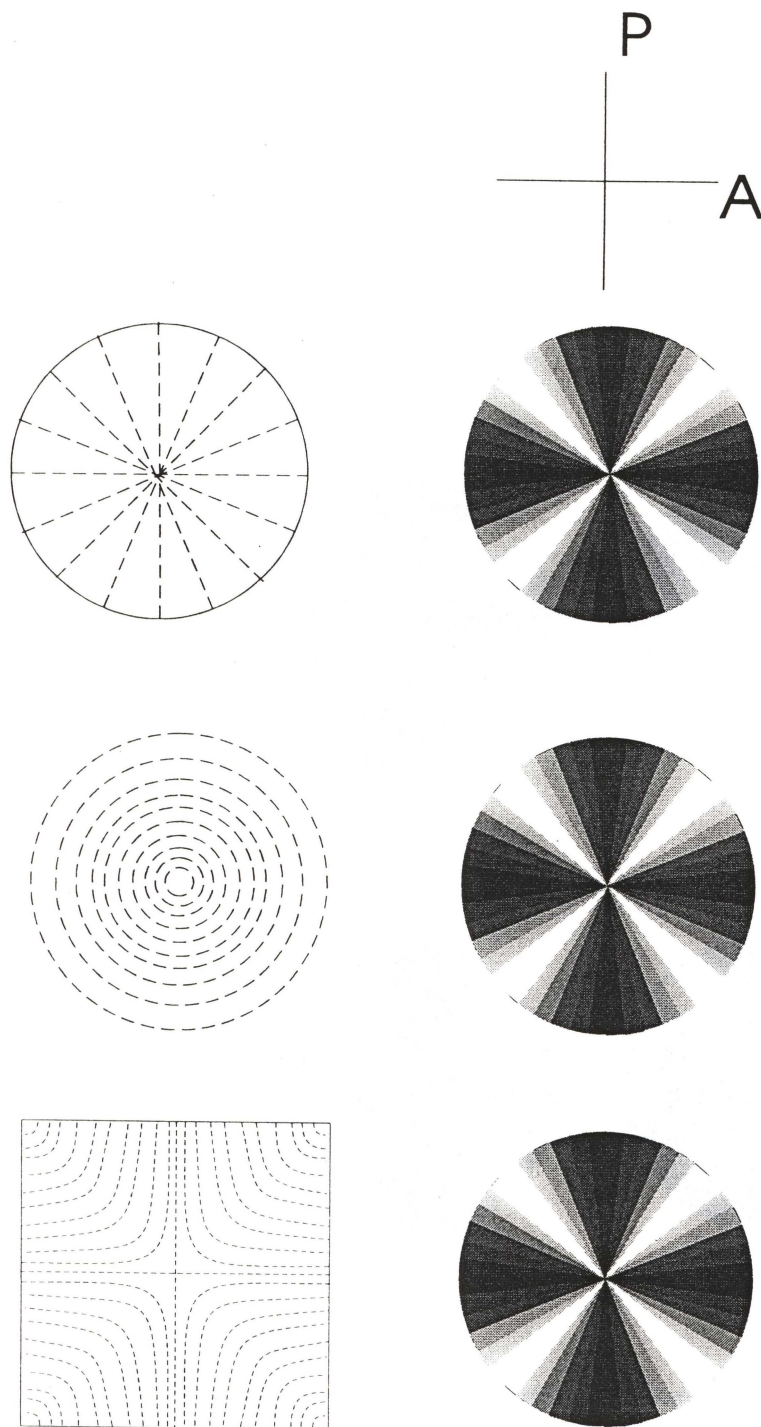


Figure 2.4: The DRLM images for different point vortices: (a) +1 splay vortex, (b) +1 bend vortex, and (c) -1 vortex.



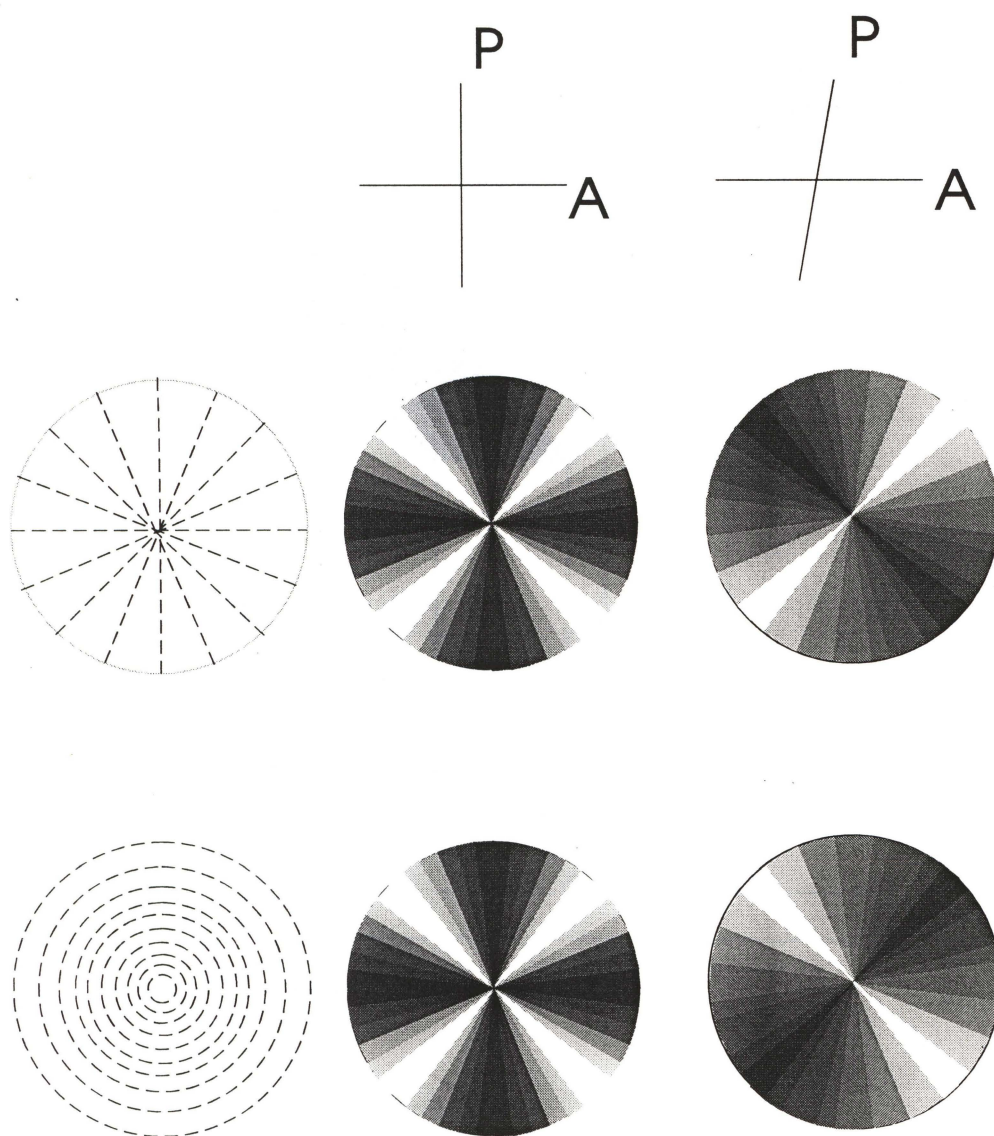


Figure 2.5: The DRLM images of splay and bend vortices under crossed and uncrossed polarizers.

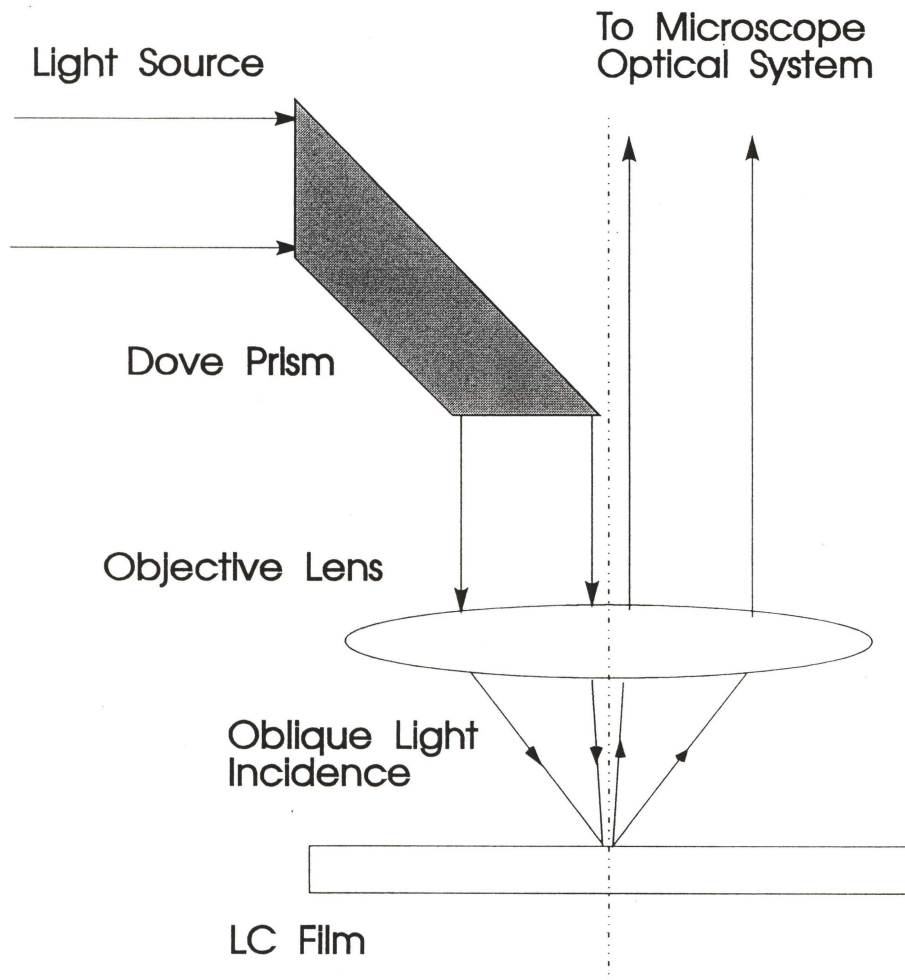
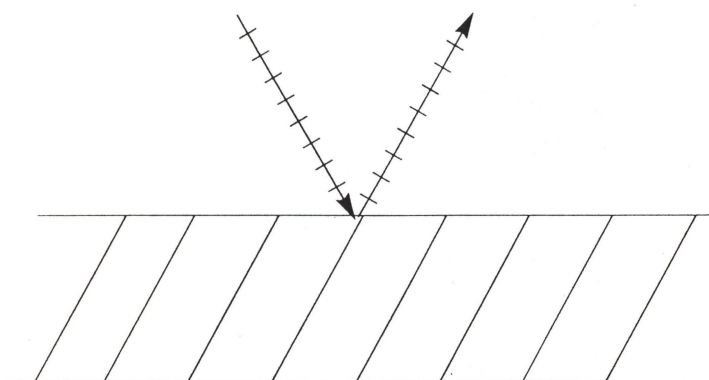
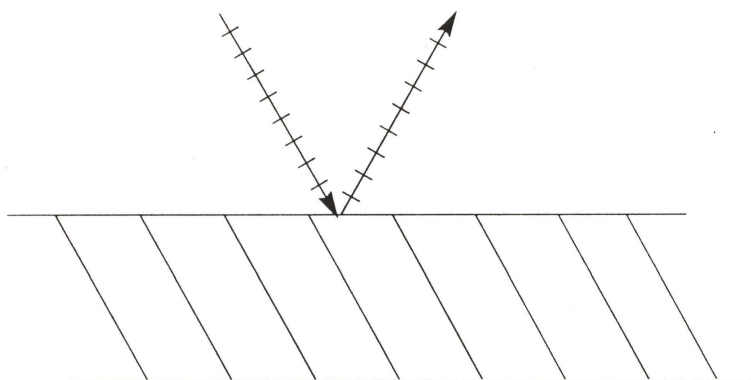


Figure 2.6: The oblique light incidence of microscope in reflection model .



(a)



(b)

Figure 2.7: The asymmetry of oblique light incidence to a tilted smectic film.  
(a) Incident light in a geometry of large reflection.  
(b) Incident light in a geometry of small reflection.

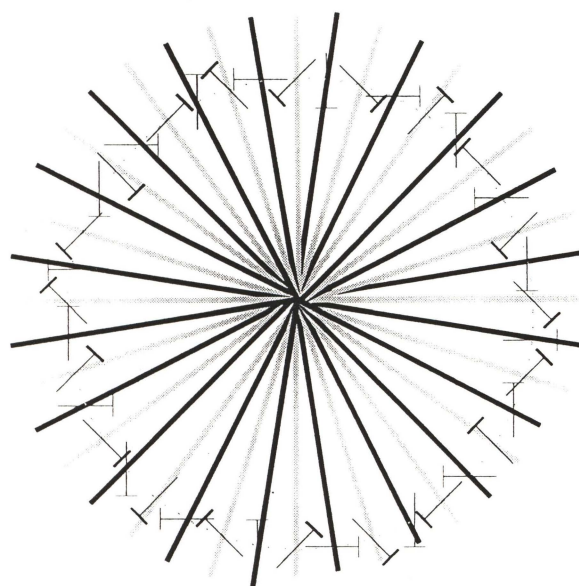
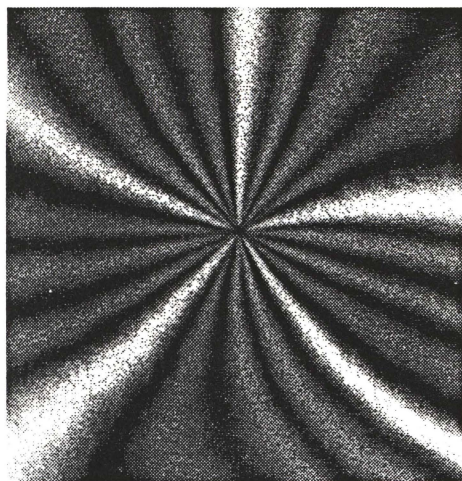


Figure 2.8: A DRLM image and c-vector field of a -5 vortex. 18-layer (+)DOBAMBC film at  $T=61^{\circ}\text{C}$ .

## CHAPTER III

### STRING DEFECTS IN FSLCFs

#### 3.1 Summary

Line (string) defects at which the molecular orientation changes by  $0, \pi/2$ , or  $\pi$  radians are reported in few layer thick tilted smectic FSLCFs. These defects are ubiquitous, appearing in chiral and nonchiral smectic C, hexatic, and antiferroelectric phases, either forming closed loops or terminating in fractionally charged vortices. The interaction between strings is complex, there being many ways in which they link to form multiarm (3 to 7) “star” and “tree” textures.

#### 3.2 Introduction

Visualization of the 2D molecular orientation field of few layer thick freely suspended tilted smectic films[9] has revealed two characteristic topological defect structures: the point ( $\pm 2\pi$ ) vortices of charge  $\pm 1$  in smectic C films[10] ; and the five- [11] and six-arm[12] star defects in tilted hexatic smectic films, in which  $+2\pi$  vortices are modulated by line defects attributed to the interaction of the molecular orientation with an underlying hexatic lattice. In this chapter we report a variety of novel 2D line (string) defects and consequent fractionally charged point defect structures in ultrathin tilted smectic films. These structures are ubiquitous, appearing in all tilted smectic films



studied, including smectic C, hexatic and antiferroelectric phases. Our observations show that the range of possible defect structures in these films is considerably broader than previously realized, indicating the presence of additional stabilization mechanisms for 2D line defects and opening the way for study of string structures in 2D XY systems.

### 3.3 Observations of string

We have studied few layer thick freely suspended films in which the local mean molecular long axis, given by the director  $\mathbf{n}$ , is tilted relative to the layer and film plane normal through an equilibrium angle  $\theta$ [9]. The projection direction of  $\mathbf{n}(x,y)$  onto the film plane defines the 2D “c director” unit vector field,  $\mathbf{c}(x,y)$ , shown in Figure 3.1(a), which can be completely described by its scalar azimuthal orientation  $\phi(x,y)$  and visualized using Depolarized Reflected Light Microscopy (DRLM) [10]. The  $\mathbf{c}(x,y)$  structures we describe here are obtained in films of uniform thickness of fewer than five layers. Thus, they are two dimensional, i.e.  $\mathbf{c}$  is uniform through the film at a given  $x,y$ , except possibly for core regions of dimension of the film thickness, distinguishing them from the 3D disclination structures of Meyer and Pershan [13] and MacLennan[14]. Films were drawn over a 3mm x 10mm hole in a glass cover slip in a hot stage with 0.01K temperature stability and DRLM carried out using a Zeiss ULTRA-PHOT microscope with a 200W high pressure mercury lamp as a light source. Film thickness was determined by optical reflectivity. The hotstage was closed with tilted double windows on the top and bottom to minimize internal thermal gradients. Because the liquid crystal molecules are optically anisotropic, the polarization vector for light reflected from a film will be rotated a few degrees toward  $\mathbf{c}$  relative to the incident-light polarization[10]. The film image

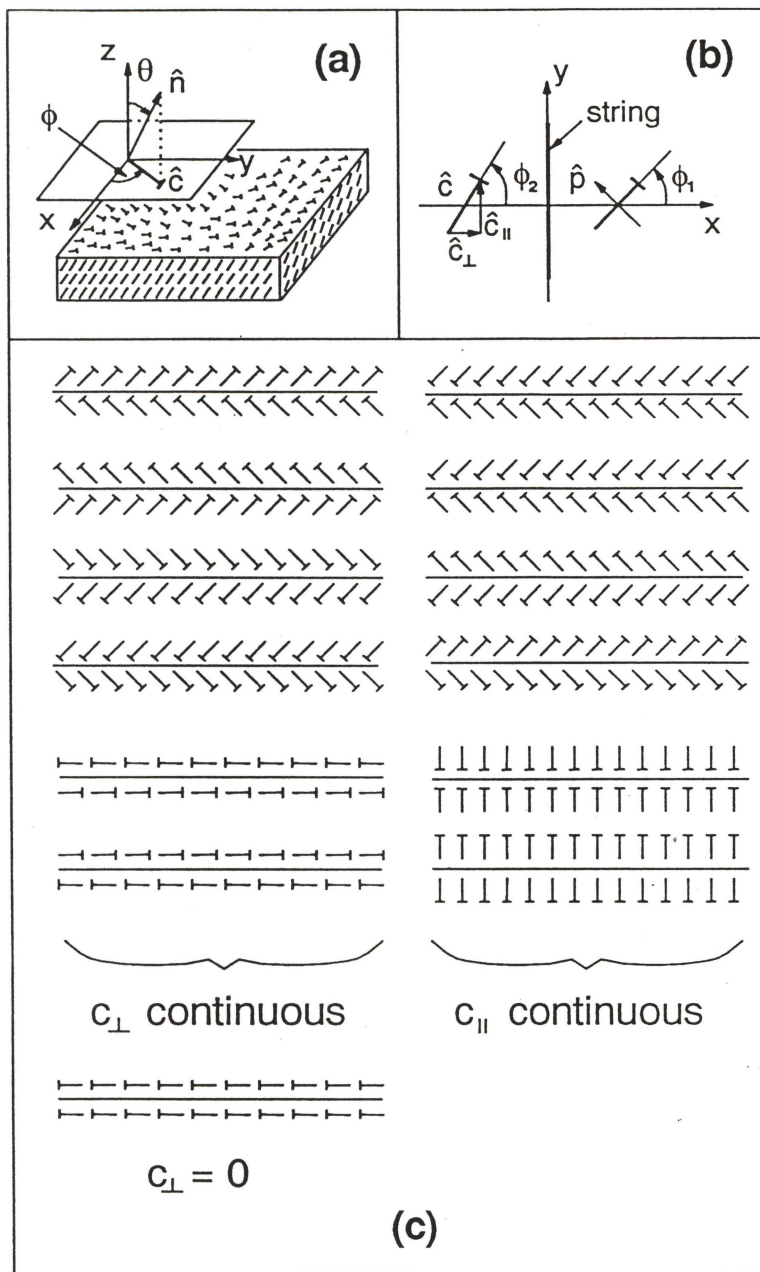


Figure 3.1: (a) Freely suspended tilted smectic film geometry. The molecular orientation is described by a vector  $\hat{n}$  with a fixed tilt angle  $\theta$  from layer normal and a variable azimuthal orientation  $\phi$ .  $\hat{c}(x,y)$  is a projection of vector  $\hat{n}$  on layer plane, the small bar indicating the end of the molecule closest to the reader. (b) Geometry of the orientation change upon crossing a string. (c) The possible  $s = 1/4$ ,  $s = 1/2$ , and  $s = 0$  strings. Only the strings in the left column have been found in our experiments.

in DRLM is thus marked by dark brushes where  $\mathbf{c}$  is parallel or normal to the incident polarization and by bright brushes when  $\mathbf{c}$  is at the intermediate ( $\pi/4$ ) orientations[10]. With normally incident light, by slightly uncrossing the analyzer[10], the spatial variation of  $\mathbf{c}(x,y)$  can be mapped modulo  $\pi$ . With oblique incidence  $\mathbf{c}(x,y)$  can be uniquely mapped.

With crossed polarizers and normally incident light, point topological defects (vortices) appear in DRLM as alternating dark and bright brushes emanating from a point (resolution limited) singularity[10]. The vortex strength  $s$ , defined as  $s \equiv \Delta\phi/2\pi$ , where  $\phi$  is the angular change in  $\phi$  on a closed path enclosing the point, can be determined since  $|s| = (\text{number of brushes})/4$ , where  $s$  has a positive (negative) sign when the brushes rotate in the same (opposite) direction as a simultaneously rotated crossed polarizer and analyzer.

String defects are sharp (resolution limited) lines across which  $\mathbf{c}(x,y)$  exhibits a discontinuous change, which may be in orientation,  $\delta\phi = [\phi_2 - \phi_1]$ , c.f. Figure 3.1b, characterized by the strength  $s = |\delta\phi|/2\pi \leq 1$ . String strength  $s$  can be determined by the behavior of the extinction brushes as the polarizers are rotated. The strings may also be characterized by the components of  $p = z \times c$ . The strings which we have found appear to satisfy the following basic rule: *As the string is crossed,  $c_{\perp}$  and  $p_{\parallel}$  are continuous while  $c_{\parallel}$  and  $p_{\perp}$  either change sign, ( $\phi_2 = -\phi_1, s = 1/4, 1/2$ ), or are zero ( $\phi_2 = \phi_1 = \pi/2, s = 0$ ).* The possible  $s = 0, 1/4$ , and  $1/2$  strings satisfying this rule are shown in Figure 3.1c. The line discontinuities of the previously observed five-fold[11] and six-fold[12] star defects are  $s = 1/6$  strings, i.e. have  $\phi = \pi/3$ .

We report here the first observation in tilted smectic films of  $s = 0$  strings, which are always in the form of closed loops, and of  $s = 1/4$ , and  $1/2$  strings which can be of finite length terminated by noninteger strength vortices and which can form complex fractal aggregates. We have studied



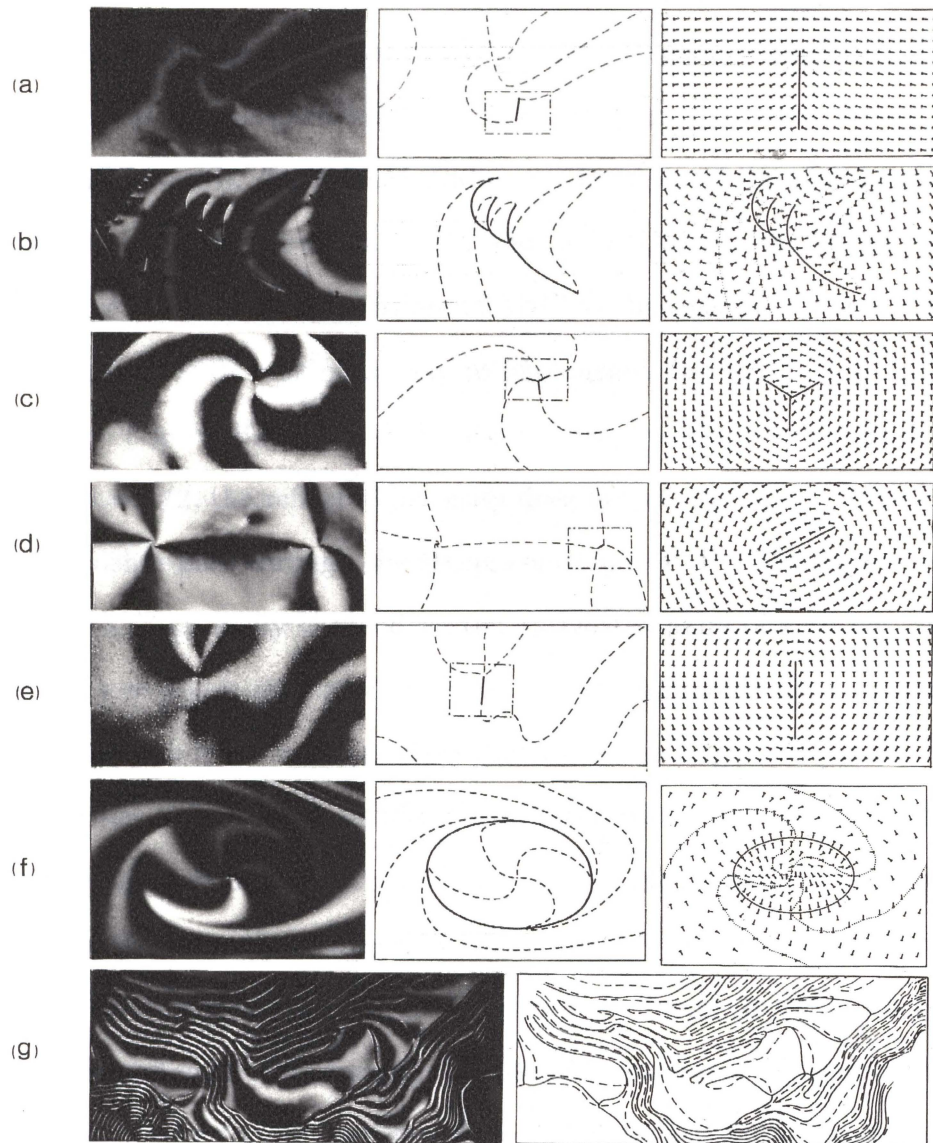


Figure 3.2: A selection of common string structures. The photographed regions are  $200\mu m$  across.

many materials and have found strings in all of them in the smectic C and tilted hexatic smectic I and F phases, including chiral, chiral-racemic, and nonchiral smectic Cs, so that string formation is not a consequence of chirality (ferroelectricity) in these systems. Usually, there are no strings in newly made films. It takes a time ranging from seconds to hours for strings to grow from the edge of the film or to spontaneously appear in regions of uniform thickness and orientation of  $c$ . Figure 3.2 presents a selection of common string structures, showing for each: the DRLM photo; a schematic of the photo indicating the strings (—) and brushes (.....); and, for (a) to (f), the underlying pattern of  $c(x,y)$ . Most of the photos are of MHTAC because this material has a large tilt angle  $\theta \cong 50^\circ$  making it easy to photograph through crossed polarizers.

Figures 3.2 (a) and (b) show examples of  $s = 1/4$  strings for which, since  $\phi = \pi/2$ , the reflected intensity does not change upon crossing the string and brushes pass through the string continuously. Finite isolated strings, ending with fractionally charged vortex-antivortex pairs of zero net charge, such as the  $s = +1/4, -1/4$  pair in Figure 3.2(a), commonly appear spontaneously in initially uniform regions. Note that the same single dark brush is linked to both ends of the string. In all cases found to date the fractionally charged vortices ending strings are of the bend type, i.e have predominately bend rather than splay distortion. Figure 3.2(b) shows a common aggregation of strings into a tree-like structure of zero net vortex charge. In this structure the region around each vertex where the strings connect has the symmetry of a “Y”, with  $p_{\parallel}$  directed away from the vertex along one string and toward the vertex on the other two (the “arms” of the “Y”, separated by  $\sim \pi/3$  radians). The region between the arms of the “Y” has primarily bend distortion in  $\mathbf{c}$  and is compressed to make a tighter distortion than the other two equivalent primarily splay regions. The predominance of bend distortion in  $\mathbf{c}(x,y)$  around the



strings is presumably a result of the typically smaller bend elastic constants in smectic C films[16].

A common defect in  $\mathbf{c}(x,y)$  is the  $s = 1$  vortex, which is found to combine with strings to form various kinds of “star” defects having 3 to 7 accompanying strings. Figure 3.2(c) shows three  $s = 1/4$  strings connected to form a three-armed star defect with a net  $s = 1$  vortex strength. Comparing this vertex where the strings meet with those in Figure 3.2(b) we find that in this structure the strings are all identical ( $p_{\parallel}$  directed toward the vertex on all three strings), making  $\mathbf{c}(x,y)$  threefold symmetric about the vertex, with an identically bend distortion between each pair of strings. Figure 3.2(d) shows a  $s = 1/2$  string ending with two  $s = 1/2$  vortices, there being two brushes linked to the each end of the string. This structure is metastable and will eventually decay to a stringless  $s = 1$  vortex. Figure 3.2(e) shows a  $s = 1/4$  string with a  $s = +1/4$  vortex on one end and a  $s = +3/4$  vortex on the other end. It will also decay to a unit-charge vortex.

Figure 3.2(f) shows what is perhaps our most remarkable observation, an  $s = 0$  string in a uniform thickness (5 layer thick) 8OSI film in the smectic C phase, in the form of a loop trapping a  $s = 1$  vortex. The brushes leaving the singularity end at the top, bottom, left and right points of the loop, indicating that  $\mathbf{c}$  is everywhere normal or parallel to the string and uncrossing the polarizer eliminates the latter possibility. Oblique incidence removes the degeneracy of the reflected light for  $\pi$  rotations in  $\phi$ , making one of the brushes leaving the defect brighter than the others. It maintains this brightness as it crosses the line defect and passes through the upper right hand corner of the photo. Thus the orientation of  $\mathbf{c}(x,y)$  is locally normal to the string and locally in the same direction on its two sides, i.e.  $\mathbf{c}$  is continuous across the defect line. Inspection of the  $\mathbf{c}$  director distribution shows that opposite preferred

sign of the splay of  $\mathbf{c}$  appears to be the principal distinction between the inside and outside of the loop. The sharp breaks in brush orientation at the string indicate the rigidity of the string and the orientational binding of  $\mathbf{c}(x,y)$  at the string. The equilibrium thermal behavior of  $s = 0$  strings will be discussed in Chapter V[6].

Figure 3.2(g) shows a massive tree-like structure of strings which commonly appears in smectic C films, coexisting with a stringless smectic C. This structure can be characterized by the string strength, in this case  $s = 1/4$ , and by the average distance between strings, which can vary from submicrons to hundreds of microns for different materials and conditions. A striking feature of the extended string structure is the absence of the spectacular orientation fluctuations in  $\mathbf{c}$  which characterize smectic C thin films[9, 10, 14, 15], indicating the orientational binding of  $\mathbf{c}$  at the string and the string rigidity. Each segment of string appears to be in local equilibrium with  $\mathbf{c}(x,y)$ , so we expect  $\phi_1$  and  $\phi_2$  to minimize a local energy  $F(\phi_1, \phi_2)$  per unit length of string. If the two air-LC surfaces of the film are identical, then  $F(\phi_1, \phi_2)$  is symmetric under  $\pi$  rotations about x, y, and z, ( $\pi_x, \pi_y, \pi_z$ , c.f. Figure 3.2b) and, if the material is nonchiral, under mirror reflection (m). If the forces coupling  $\phi_1$  and  $\phi_2$  across a string are sufficiently weak we may write  $F(\phi_1, \phi_2) \sim f(\phi_1)f(\phi_2)$  and invariance under  $\pi_x, \pi_y, \pi_z$  requires that  $f(\phi)$  be symmetric about  $\phi = 0, \pi/2$ , and  $\pi$ . This produces  $s = 1/2$  strings if  $f(\phi)$  has a minimum at  $\phi = \pi/2$ , and  $s = 1/4$  strings if  $\phi = 0, \pi/2$ , and  $\pi$  are maxima and the dominant contribution to  $f(\phi)$  is the lowest compatible Fourier component in  $\phi$ .

### 3.4 The 2D XY models and strings

The 2D polar nematic order of  $\mathbf{c}(x,y)$  can be usefully modelled as a 2D XY system, and there have been several theoretical explorations of string-like structures in the 2D XY model, based on introducing local interactions which reduce the core energy of vortices[17, 18]. Our observation of isolated well-defined one-dimensional defect lines supports this approach.

Lee and Grinstein [17] considered the isotropic XY Hamiltonian

$$H = - \sum_{\langle i,j \rangle} [\Delta \cos(2\delta\phi_{ij}) + K \cos(\delta\phi_{ij})], \quad (3.1)$$

which has a combination of polar nematic and nonpolar nematic nearest neighbor interactions, and  $\langle i, j \rangle$  represents nearest-neighbor pairs. Here  $0 \leq \phi_i \leq 2\pi$  is the angle that the spin at site  $i$  makes with some fixed axis, and  $\delta\phi_{ij} \equiv \phi_i - \phi_j$ . When  $\Delta \geq K/4$ , the above potential has a metastable minimum at  $\phi = \pi$ , which lies  $2\Delta$  in energy above the absolute minimum at  $\delta\phi_{ij} = 0$ . Ising-type excitations of the perfectly ordered ferromagnetic ground state consisting of groups of spins overturned by  $\pi$  are then metastable and there are, in addition, excitations not present in Ising models, namely, one-dimensional strings of antiparallel spins that terminate in half-charge vortices as shown in Figure3.3.

Swendsen [18] considered the Hamiltonian

$$H = H_1 + H_x = -K \sum_{\langle i,j \rangle} \vec{\sigma}_i \cdot \vec{\sigma}_j - K_x \sum_{\text{plaquettes}} (1 - \vec{\sigma}_i \cdot \vec{\sigma}_k)(1 - \vec{\sigma}_j \cdot \vec{\sigma}_l), \quad (3.2)$$

where  $\vec{\sigma}_i$  is classical, two-dimensional spin of unit length on a square lattice. In addition to  $H_1$ , the usual XY interaction, H contains  $H_x = K_x S_x$ , in which under the ‘‘crossed-product’’ operator  $S_x$ , the corners of a plaquette are labeled sequentially with  $i, j, k$ , and  $l$  and each scalar product involves spins at opposite corners of a plaquette. The operator does not affect the harmonic term in a

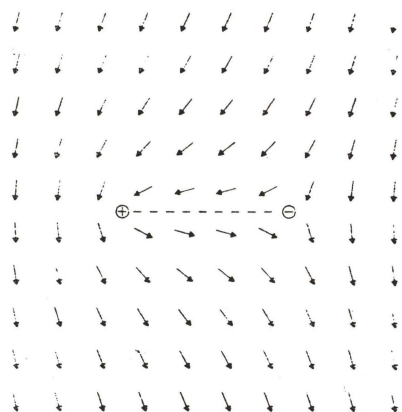


Figure 3.3: A half-integer vortex-antivortex pair connected by a string. The centers of the half-integer vortices are represented by the circles around the plus and minus signs, and the string is represented by the dashed line.

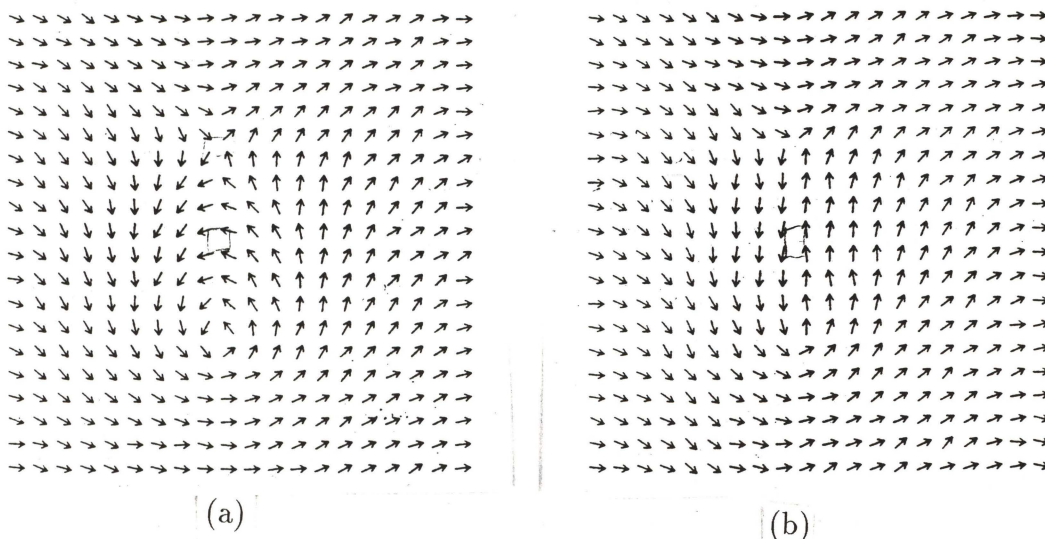


Figure 3.4: Monte Carlo simulation of string defect. (a)  $20 \times 20$  spin configuration with a vortex-antivortex pair. (b) Starting with (a), 40 MC steps/site at  $K_1 = 20.0$  and  $K_x = 9.5$  produced a vortex-antivortex pair with charge one-half. Tracing a path around a half-vortex, the spin rotate only 180 deg.



expansion of the Hamiltonian for small fluctuations and only couples to spin waves in higher order. Starting from a vortex-antivortex pair, a very short Monte Carlo run with some appropriate choices of positive  $K$  and  $K_x$  produced  $\pi$ -strings terminated by half-charge vortex-antivortex pairs as shown in Figure 3.4. The vortex-antivortex interaction potential included a logarithmic term with effective charge one-half, and a linear term (confinement) due to the connecting line of plaquettes with reversed spins.

Since the string defects are stabilized by strong local interaction, we propose that a 2D string system is a conformal mapping from a normal XY system. For example,

$$G(z) = Ze^{i\frac{\pi}{2}} \quad (3.3)$$

represents a +1 bend vortex at  $z=0$  in a XY-model. The conformal mapping

$$W = \frac{1}{2}\left(Z + \frac{1}{Z}\right) \quad (3.4)$$

can map a +1 vortex into a pair of  $+\frac{1}{2}$  vortices with an  $s=1/2$  string links them [Figure 3.5].

These theoretical models show that string-like defects can be stabilized by sufficiently strong local interactions favoring adjacent regions of differing orientation of  $\mathbf{c}(x,y)$ . However, the prevailing notions of molecular interaction and elasticity in liquid crystals offer no ready origin for such interactions. Additionally, our observation of  $s = 0$  strings suggests that the strings are some local structure atypical of liquid crystals. The strings we report here differ in a significant way from those of the models in that in the models the strings are in thermal equilibrium, with the density of strings being a strong function of temperature. In the films the strings appear and grow gradually at a fixed temperature and behave as if the net string length were fixed by some nonthermal constraint. This suggests that the strings may be a result of low solubility



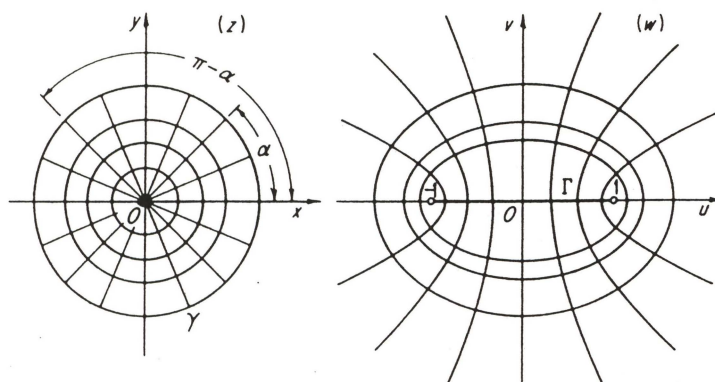


Figure 3.5: Conformal mapping of  $W = \frac{1}{2}(Z + \frac{1}{Z})$ .

impurities which aggregate in the film plane. The films have extremely large surface-to-volume ratios and tend to be rather well ordered into layers by the surface tension[19]. The former favors the accumulation of impurities and the latter may make collected impurities poorly soluble as isolated molecules in the liquid crystal. This would force the formation of aggregates which, by virtue of a larger surface tension than the liquid crystal would not simple form drops, but rather collect into lines. Purposely hydrating the films does not produce strings.

## CHAPTER IV

### A CHIRAL SYMMETRY BREAKING TWIST-BEND INSTABILITY IN ACHIRAL FSLCFs

#### 4.1 Summary

Freely suspended smectic C films, 2-, 3-, and 4-layers in thickness, of the achiral compound  $C_7F_{15}CH_2O - \phi - COO - \phi - OC_6H_{13}$  exhibit a thermotropic transition at which the uniform (2D) smectic C molecular orientation field becomes modulated by a periodic bend wave soliton. No such transition is found in single layer (1-layer) films. This transition is interpreted as a chiral symmetry breaking marking the spontaneous appearance of frustrated local bend.

#### 4.2 Introduction

Some of the most interesting structures of liquid crystal phases arise as a result of internal frustration, the situation in which the local energetically ideal configuration cannot be extended to fill space, but must be accommodated by the appearance of defects, often in periodic arrays [22]. The classic 3D examples are the blue phases, in which the optimal filling of space with the symmetry-imposed 2D twist of the local average molecular long axis orientation,  $\mathbf{n}(\mathbf{r})$ , requires a network of line or point defects [23]. Such frustration-induced modulations are also found at the smectic C - air interface in thermotropic freely suspended films [13, 14], and, recently, in Langmuir monolayers [24],

in the form of a quasi-periodic modulation of  $\mathbf{c}(x,y)$  giving the projection of  $\mathbf{n}(r)$  at the surface onto the surface plane. In these cases the head-tail polar molecular ordering at the surface induces a preference for nonzero splay of  $\mathbf{n}(r)$  and, in turn, of  $\mathbf{c}(x,y)$ , giving rise to the splay stripes which enable the preferred sign of splay everywhere on the surface[25]. Similarly, stripes having one sign of bend appear in freely suspended liquid crystal films as a result of molecular chirality[26, 27].

In these examples it is the intrinsic symmetry that favors local splay, bend, or twist of a particular sign. In this Letter we report the first observation of internal frustration and consequent spatial modulation appearing as a spontaneously broken symmetry, initially in the form of a bend wave in  $\mathbf{c}(x,y)$  of a smectic C. These structures are readily distinguished from the above examples in that while this system locally prefers bend there is no preference as to the sign of the bend, so that both signs appear equivalently. The possibility of such an instability was recently shown using a theoretical model based on a Landau free energy by Selinger, Wang, Bruinsma and Knobler (SWBK), who calculated a phase diagram having regions of 1D and 2D sinusoidal and soliton-like modulations[28]. They also point out that, since in the smectic C phase local bend implies local twist and therefore local chirality, this bend instability is a periodic chiral symmetry breaking. Here, we present clear evidence for such a thermotropic spontaneous chiral symmetry breaking transition in an achiral smectic C material.

### 4.3 Experiment and Results

Experiments were carried out on 1 to 10 layer thick freely suspended films of the achiral 3M compound CRL-EX-900084 ( $C_7F_{15}CH_2O - \phi - COO -$

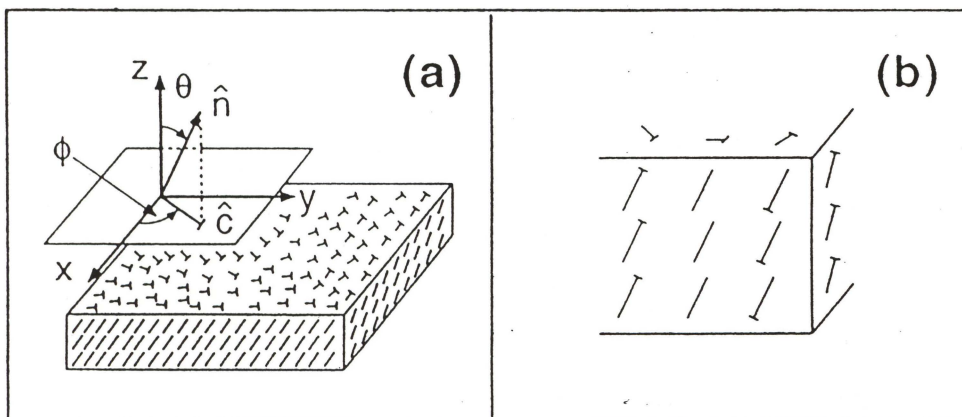


Figure 4.1: (a) Freely suspended smectic C film geometry. The mean molecular long axis orientation is described by a vector  $\mathbf{n}(\mathbf{r})$  with a fixed tilt angle  $\theta$  from layer normal. The "c director",  $\mathbf{c}(x,y)$ , the unit vector giving the projection of  $\mathbf{n}(\mathbf{r})$  on layer plane, has a variable azimuthal orientation  $\phi(x,y)$ . The "tees" give the projection of  $\mathbf{n}$  on the surfaces indicated, with the small bar on the end of the molecule closest to the surface. (b) Geometry showing that bend of  $\mathbf{c}(x,y)$  requires both twist and bend of  $\mathbf{n}(\mathbf{r})$ , and that when  $\theta$  is small the principal deformation of  $\mathbf{n}$  is twist.

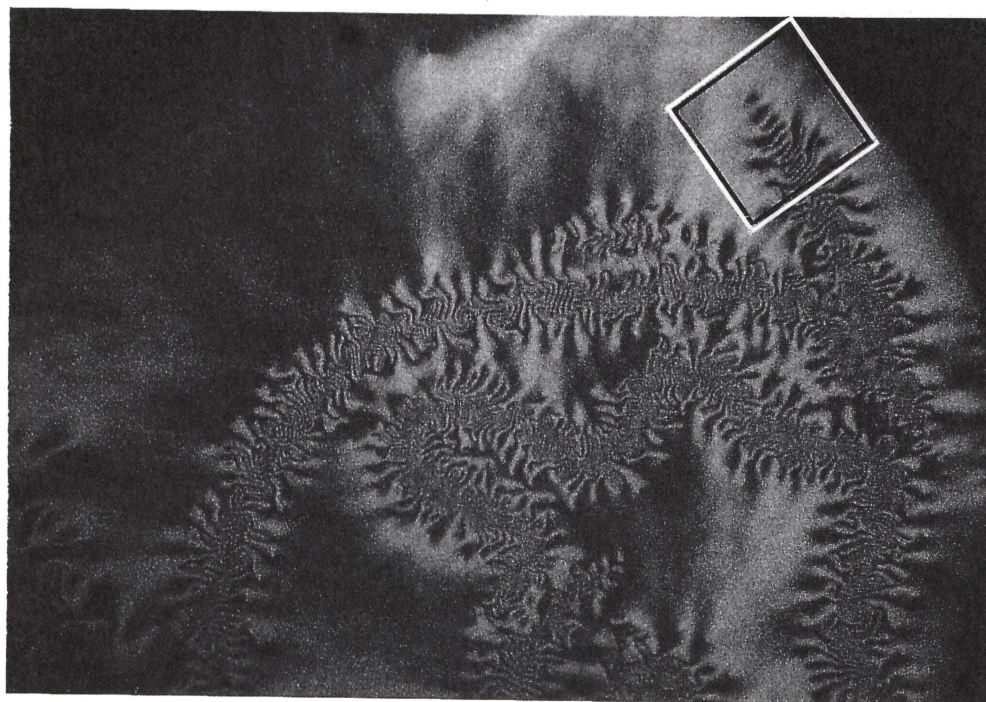
$\phi - OC_6H_{13}$  ), notable for having one aliphatic and one perfluoroalkyl chain. The bulk material has isotropic ( $I$ ), smectic A ( $Sm - A$ ), smectic C ( $Sm - C$ ), and crystal ( $K$ ) phases vs temperature  $T$  as follows:

$$I \xrightarrow{136} Sm - A \xrightarrow{79} Sm - C \xrightarrow{71} K.$$

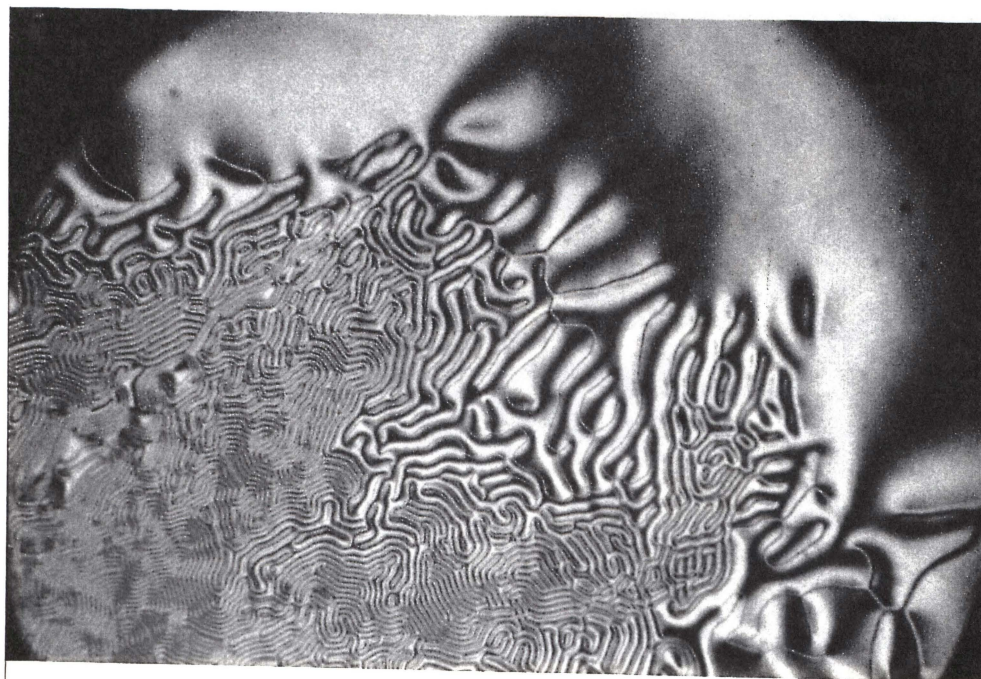
In 1 to 4- layer thick freely suspended films the crystallization transition is suppressed below  $71^\circ C$  and the smectic C can be observed to lower  $T$ . As  $T$  is decreased the films eventually break, with  $T = 65^\circ C$  the lowest achieved in a liquid crystal phase. The film geometry is shown in Figure 4.1a. The local mean molecular long axis, given by the director  $\mathbf{n}$ , is tilted relative to the layer and film plane normal through an equilibrium angle  $\theta$ [9]. The projection direction of  $\mathbf{n}(x,y)$  onto the film plane defines the 2D “c director” unit vector field,  $\mathbf{c}(x,y)$ , shown in Figure 4.1(a), having a local mean scalar azimuthal orientation  $\phi(x,y)$  which can be visualized using Depolarized Reflected Light Microscopy (DRLM)[10, 29]. Films were drawn over a  $3\text{mm} \times 10\text{mm}$  hole in a glass cover slip in a hot stage closed with tilted double windows on the top and bottom to minimize internal thermal gradients and give 0.01K temperature stability. Because the liquid crystal molecules are optically anisotropic, the polarization vector for light reflected from a film will be rotated a few degrees toward  $\mathbf{c}$  relative to the incident-light polarization [10]. The film image in DRLM is thus marked by dark brushes where  $\mathbf{c}$  is parallel or normal to the incident polarization and by bright brushes when  $\mathbf{c}$  is at the intermediate ( $\pi/4$ ) orientations[10]. Here we use oblique incidence and a slight uncrossing of the analyzer [29], to uniquely map  $\mathbf{c}(x,y)$ .

Figure 4.2 shows DRLM images of the instability as it appears upon lowering temperature in the Sm-C phase of a 4-layer thick film. The Sm-A to Sm-C transition is at  $85^\circ C$  in the 4-layer film (the Sm-A-Sm-C transition is





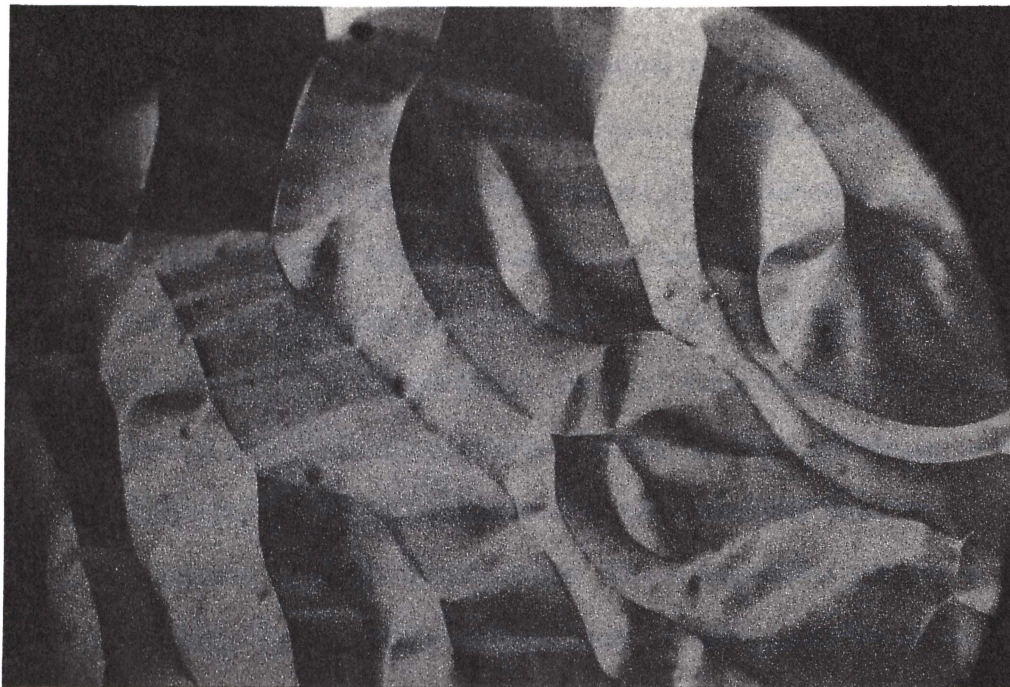
(a)



(b)

Figure 4.2: DRLM photomicrographs of CRL-EX-900084 freely suspended smectic C films. The diameter of the field is  $100\mu\text{m}$  on the film: (a) Batonnets ( $\sim 10$ ) of the bend instability appearing in the smectic C phase in a 4-layer film at  $T = 70.4^\circ\text{C}$ . The growing batonnet tip (box) is mapped in Figure 4.4(a). (b) Quasi-periodic network of string-like line defects, developing at  $T = 70.0^\circ\text{C}$  out of the batonnets in a 4-layer film. The defect textures are characteristic of those found in 2D periodic stripe systems[30, 31].





(a)



(b)

Figure 4.3: (a) Global texture obtained in a 2-layer film at  $T = 69^{\circ}C$ . This texture is found in other 2D periodic stripe systems[30, 31]. (b) Global 2D focal conic texture obtained in a 4-layer film at  $T = 69^{\circ}C$  where the local period has decreased to below the microscope resolution. Here DRLM visualizes the local stripe orientation because of the anisotropy in the average orientation of  $c$  relative to the strings. The boxed area is mapped in Figure4.1.

elevated in thin films as is usual[16]) and the Sm-C texture obtained is typical for freely suspended smectic C films: a gradual variation of  $c(x,y)$  across the film, marked by the dramatic flickering due to orientational fluctuations of  $\mathbf{c}$  [9, 10]. At  $T = 70.4^\circ C$  batonnet-like regions of spontaneous deformation of  $\mathbf{c}(x,y)$ , shown in Figure 4.2(a), nucleate at many places on the film [ $\sim 10$  in Figure 4.2(a)] and gradually grow to cover it. The boxed area of the batonnet growing tip is mapped in Figure 4.4(a). As  $T$  is further lowered the deformation evolves into a quasi-periodic network of string-like line defects, as shown in Figure 4.2(b) at  $T = 70.0^\circ C$ . This local quasi-periodicity enforces a 2D focal conic-like texture on larger length scales. The string defect spacing decreases with decreasing  $T$ , ultimately falling below  $\sim 5\mu m$ , the resolution of the microscope, and in this limit the 2D focal conic-like texture, shown at  $T = 69.0^\circ C$  in Figure 4.3(b) for a 4-layer film, and in Figure 4.3(a) at  $T = 71^\circ C$  for a two layer film, can be visualized, because of the anisotropy in the local mean orientation of  $\mathbf{c}$  relative to the local stripes. These focal conic textures bear a strong resemblance to the global textures found in other 2D systems having local periodicity[30, 31].

Since the bend of  $\mathbf{c}$  removes the  $\mathbf{z}$ - $\mathbf{c}$  mirror symmetry plane, it leaves the film locally with only a  $C_2$  axis along  $\mathbf{p} = \mathbf{c} \times \mathbf{z}$ . Thus, the bend wave produces a local chiral symmetry breaking of the initially achiral system, and there is a local ferroelectric polarization  $\mathbf{P} = \beta[\mathbf{c} \times \nabla \times \mathbf{c}]$ , along  $\mathbf{p}$ , where  $\beta$  is a constant of proportionality. Also, a necessary consequence of the chiral symmetry breaking is the twist of  $\mathbf{n}(x,y,z)$  which accompanies the bend of  $\mathbf{c}(x,y)$ , or, as we suggest below, may drive it.

Figure 4.4(a) shows a DRLM mapping of the structure of  $\mathbf{c}(x,y)$  in the vicinity of a growing tip of a batonnet of the instability in a 4-layer film (boxed area of Figure 4.2(a)). The principal distortion when the instability first



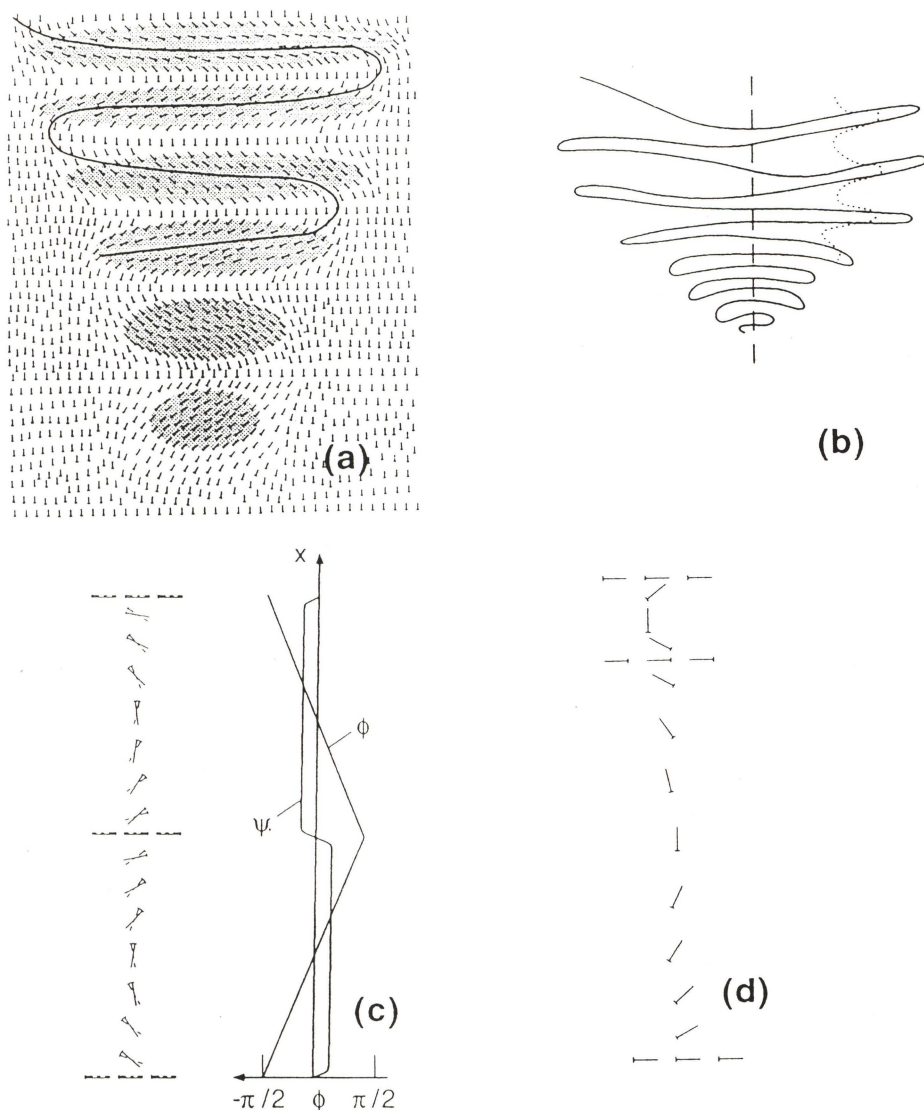


Figure 4.4: (a) DRLM map of the growing batonnet tip of Figure 4.2(a), showing that the instability is a bend wave, with positive and negative bend appearing equivalently. The fully developed instability, further into the batonnet, is soliton-like, a periodic array formed by a line defect where  $c$  is continuous (zero strength strings) and the sign of bend switches. (b) Typical geometry of the bend soliton line (zero strength string) in a growing batonnet. The dotted line indicates a contour of  $c$ . While the two signs of bend are of similar strength along the (dashed) batonnet center-line, positive bend becomes larger on the right hand side of the batonnet and vice versa, with a ratio of the bend magnitudes as large as 10:1 developing. Overall the net chirality (bend) averages to zero. (c) Schematic of the bend soliton in which positive and negative bend form equivalent structures, showing: the associated twist of  $n$ , indicated by the solid and dot-dash directors of adjacent layers; the position dependence of  $\phi(x)$ ; and the position dependence of the symmetry breaking order parameter  $\psi(x)$ . (d) Schematic of the inequivalent bend soliton, evident in Figures 4.2 (a,b).

appears is a periodic bend modulation of  $\mathbf{c}(x,y)$ , the film developing regions of nonzero  $\nabla \times \mathbf{c}$ , which periodically changes sign in a 1D wave-like pattern. The regions of opposite sign of bend initially occur equivalently, the instability appearing to simply favor finite bend, without selection with respect to its sign. *It is important to note that all of these changes occur within the smectic-C phase, that is, there is no evidence that they are a result of transitions to more ordered smectic-F, -I, or -L phases.* As the batonnet grows, the bend modulation increases in amplitude, developing into distinct stripes having a boundary line, shown as the solid line in Figure 4.4(a), at which the sign of bend abruptly changes, i.e. at which the bend amplitude evolves from a “sinusoidal” to a “square wave” soliton-like periodic spatial dependence. Note that  $\mathbf{c}(x,y)$  is locally parallel to the stripe boundary and does not change in orientation as it is crossed, i.e. the boundary line is an “ $s = 0$  string”, as first identified by Pang et al. [29], marking only the change in preferred sign of bend. Figure 4.4(b) shows the typical larger scale structure of the bend soliton line in a developing batonnet and Figure 4.4(c) the 1D bend soliton structure obtained from the SWBK model along with its corresponding  $\phi(x)$ . The qualitative match to the observed deformation is very good, with the important exception that maximum magnitude of the bend in the regions of opposite bend sign can be inequivalent in the soliton regime. This is evident in Figures 4.2(a) and 4.2(b), especially in the interfacial region between the modulated and uniform phases, and shown schematically in Figures 4.4(b) and 4.4(d). The ratio of maximum bend magnitudes in the regions of opposite sign can be as large as  $\sim 10 : 1$ . While this indicates a local predominance of one chiral sign, the global average of the chirality appears to be zero, as shown for the batonnet in Figure 4.4(b), where the two signs of bend dominate similarly but in different regions.



This bend instability is found in 2,3, and 4-layer films. In 5-layer and thicker films crystallization preempts the instability upon lowering  $T$ , with elongated crystallites growing out onto the film from the edge before the instability can occur upon lowering temperature. It is possible to make 1-layer films of this material. These remain in the uniform smectic C texture for  $T > 65^\circ C$ . Thus the instability, if it occurs at all in 1-layer films, is strongly suppressed, although, as indicated below, we have good reason to expect that the instability will not be found at all in 1-layer films. The temperatures for the onset of the instability in 1 to 4-layer thick films are  $T_1 < 65^\circ C$ ,  $T_2 = 71.5^\circ C$ ,  $T_3 = 68.8^\circ C$ , and  $T_4 = 70.4^\circ C$ , exhibiting an odd-even oscillation in the onset temperature. The instability exhibits some thermal hysteresis.

The localized batonnet-like nucleation of the instability, the coexistence of unmodulated and modulated phases, and the hysteresis indicates onset behavior analogous to that of a first order phase transition. However, as for other first order liquid transitions such as the nematic-isotropic, two phase coexistence [c.f. Figure 4.2(a,b)], and thermal hysteresis indicate the presence of a low concentration of impurities having different solubility in the unmodulated and modulated phases.

#### 4.4 Theory

Several qualitative features of this transition can be understood from the SWBK free energy:

$$F = \int d^2r \left[ \frac{1}{2}K_s(\nabla \cdot c)^2 + \frac{1}{2}K_b(\nabla \times c)^2 - \lambda\psi(\nabla \times c) + \frac{1}{2}\kappa(\nabla\psi)^2 + \frac{1}{2}t\psi^2 + \frac{1}{4}m\psi^4 \right] \quad (4.1)$$

Here  $K_s$  and  $K_b$  are the Frank elastic constants for splay and bend, respectively, and  $\lambda$  is the constant that determines the coupling of bend to the symmetry

breaking order parameter  $\psi$ . The second term is a Landau free energy which generates the appearance of  $\psi$ .

Comparing our results to the predictions of the SWBK model [28], we are qualitatively in the region of their phase diagram where sinusoidal stripe, square lattice, and soliton regions are successively encountered upon lowering T. As expected from the model the stripe periodicity decreases with decreasing T, indicating an increasing amplitude of  $\psi$ . The model predicts that as T is further decreased an increase and divergence of the periodicity to form a uniform chiral phase, a consequence of the increasing energy cost of spatial gradients of  $\psi$ . We do not observe such a divergence, possibly indicating that  $\kappa$  is small, although the T-range where the modulated phase is accessible is rather narrow.

#### 4.5 Discussion

We now consider the physical origin of the symmetry breaking in this system. As noted above, bend of  $\mathbf{c}(x,y)$  is accompanied by both twist of  $\mathbf{n}(\mathbf{r})$ ,  $|\mathbf{n} \cdot \nabla \times \mathbf{n}| = \sin \theta \cos \theta |\nabla \times \mathbf{c}|$ , and bend of  $\mathbf{n}(\mathbf{r})$ ,  $|\mathbf{n} \times \nabla \times \mathbf{n}| = \sin^2 \theta |\nabla \times \mathbf{c}|$ . Since the tilt angle  $\theta \sim 25^\circ$  is small, the deformation of  $\mathbf{n}(\mathbf{r})$  predominately twist, and, as Figure 4.1(b) shows, this twist is largely *intralayer*. The absence of the instability in single layer films then points to an important role for physical differences between layers in single vs. multiple layer films. An obvious difference is that the single layer film must be on the average *apolar* with respect to end-for-end molecular orientation, whereas the surface layers in multiple layer films are necessarily polar [32, 33]. Further evidence for polar ordering at the surface is found from the surface energy, which is lower for films having even numbers of layers than that of films with odd numbers of layers, indicating

a preference for polar surface ordering, a result of the amphiphilic character of this molecule [34].

These observations suggest an instability mechanism favoring twist of  $\mathbf{n}(\mathbf{r})$  in polar ordered layers of this material, which we suggest originates as a result of the strong difference of the opposing perfluoro and perhydro alkyl tails. The fluoro tail has a much greater stiffness, owing to the steric hindrance of the fluorine atoms which produces a rigid helical chain, and has a cross-sectional area  $\sim 1.27$  times that of perhydrogenated one[35]. The polar ordering generates a fluoro-core-hydro trilayer substructure within each smectic layer. The large fluoro chain area and entropic pressure tending to increase the area per molecule in the hydrocarbon tail[36] make this structure have the character of a packing of dumbbell-shaped objects, in which the cores (center regions) can be brought closer together if there is a twist between nearest neighbors.

We proposed the possible film structures as shown in Figure 4.5. For a whole film, it is an apolar film, but, it may contain polar layers. In the case of monolayer film, there is only one apolar layer. We have not seen the bend-twist instability in a monolayer film at any temperature. For a two-layer film, it may consist of two polar layers with opposite polar directions. This structure can produce a larger twist force upon LC molecules. For a three-layer film, it may contain two polars at its two surfaces and an apolar layer in the middle. The center apolar layer may cut down the twist force. For a four-layer film, it may contain two bilayers.

monolayer film



Two-layer film  $T_c = 71.5^\circ\text{C}$



Three-layer film  $T_c = 68.8^\circ\text{C}$



Four-layer Film  $T_c = 70.4^\circ\text{C}$



Figure 4.5: Bilayer structures of films. Apolar films may contain polar layers. (a) Monolayer film, (b) Two-layer film, (c) Three-layer film, and (d) Four-layer film.



## CHAPTER V

### A NOVEL SPLAY INSTABILITY IN FSLCFs

#### 5.1 Summary

A novel splay stripe phase is observed in thin and uniform, freely suspended smectic-C liquid crystal films of compounds 8OSI, DOBAMBC, 7O.7, etc. The  $c$ -vectors are in splay deformation inside stripes, and there is an alternation of splay signs between successive stripes. The boundaries of stripes are “ $s=0$  strings”, and the  $c$ -vectors are perpendicular to them. The film starts in a low temperature domain separation phase, then upon heating, the “ $s=0$  strings” change from straight lines to sinuous lines and gradually the film turns into a stripe phase. This phenomenon is a clear indication of polar symmetry breaking in the films. We have measured the temperature dependence of the splay stripe width, and it agrees our theory very well.

#### 5.2 Introduction

There is currently a great deal of interest in domain shapes as they are common phenomenon in a wide variety of 2D and 3D physical and chemical systems[38]. Liquid crystals, especially freely suspended liquid crystal films, are rich in symmetry breaking and phases. These films are among the best systems to study 2D domain properties. Some of the 2D domain structures, like Langmuir monolayers[12] and freely suspended liquid crystal smectic



films(FSLCFs)[6, 28], arise as a result of spontaneous chiral- symmetry breaking in 2D systems of achiral molecules. Recent experiments show a twist-bend instability in achiral FSLCFs[6]. At high temperature, the film is in a uniform smectic-C phase. Upon cooling, the c-vectors form 2D sinusoidal bend patterns with an alternation of bend signs between successive stripes. Further cooling causes those patterns to become solitonlike stripes. The boundaries of the stripes are “ $s=0$  strings” with the c-vectors parallel to the strings. This phase transition is mainly driven by the interior twist field in polar ordered layers of the material, which has a rigid fluoro tail. This twist-bend instability can be understood by the theoretical model of Selinger, Wang, Bruinsma, and Knobler(SWBK)’s[28] which is based on a local chiral order parameter and its coupling to bend deformations of the c-vector.

Another stripe structure is the splay stripe. Frank[39] has demonstrated through symmetry arguments the intrinsic relationship between splay strains and the polarization in liquid crystal. He shows that if there is an intrinsic polarity in the molecular ordering of a liquid crystal, then that liquid crystal in its lowest energy structure will tend to be uniformly splayed and ferroelectric. Since no continuous 3D or 2D structures can contain uniform splay, this polar liquid crystal would have a fine domain structure, with approximately optimum splay in each domain, and would be space charged as well as surface charged. Meyer[5] extends Frank’s ideal to a nonpolar liquid crystal which is neither spontaneously splayed nor ferroelectric, but either splay or polarization is externally induced in the structure by mechanical stress or an electric field, respectively. By changing the symmetry of the system from nonpolar to polar, the presence of splay will then induce polarization, or vice versa. This explains the stripe- like domain pattern with alternating regions of splay and bend found in a nematic cell when a moderate electric field is applied[40]. In

FSLCFs, the asymmetric environment of the surface can induce a polar asymmetry in the distribution of molecular orientations near the surface[13]. Meyer and Clark[13] show that the splay domains in the surfaces of FSLCFs are separated by surface disclinations at which  $\theta$  changes discontinuously. In Langmuir monolayers, the head-tail polar molecular ordering at the surface induces splay stripes which also have surface disclinations[12, 37].

### 5.3 Polar symmetry breaking in FSLCFs

We report the first observation of a splay instabilities and polar phase separations in thin uniform FSLCFs. The splay domains in these films are separated by “s=0 strings” . The film geometry is shown in Figure 5.1(a-b). The local mean molecular long axis, given by the *vector*  $\mathbf{n}$  for polar molecules or by the *director*  $\mathbf{n}$  for non-polar molecules, is tilted relative to the layer and film plane normal through an equilibrium angle  $\theta$ . The *c-vector* is defined as the projection of the *director*  $\mathbf{n}$  and indicated by a “tee” symbol in which the small bar shows which end of the molecules is closest to the surface. A given c-vector can represent either of two possible antiparallel orientations of the respective polar molecule[Figure 5.1(b)]. In order to distinguish those two cases, a 2D polar vector or *p-vector* is defined as the projection of the *vector*  $\mathbf{n}$  on the layer plane as indicated by the arrows in Figure 5.1. Using depolarized reflected light microscopy(DRLM), only the c-vector field  $\mathbf{c}(x,y)$  can be visualized[10]. For an ultra-thin film made up of polar molecules, there are two equivalent polar phases depicted as phases I and II in Figure 5.1(b). In phase I the *c-vector* and *p-vector* are *parallel* to each other, in contrast to phase II where the *c-vector* and *p-vector* are *anti-parallel* to each other. For a given polar liquid crystal molecule, the tendency to splay is fixed relative to the *vector*  $\mathbf{n}$  or the

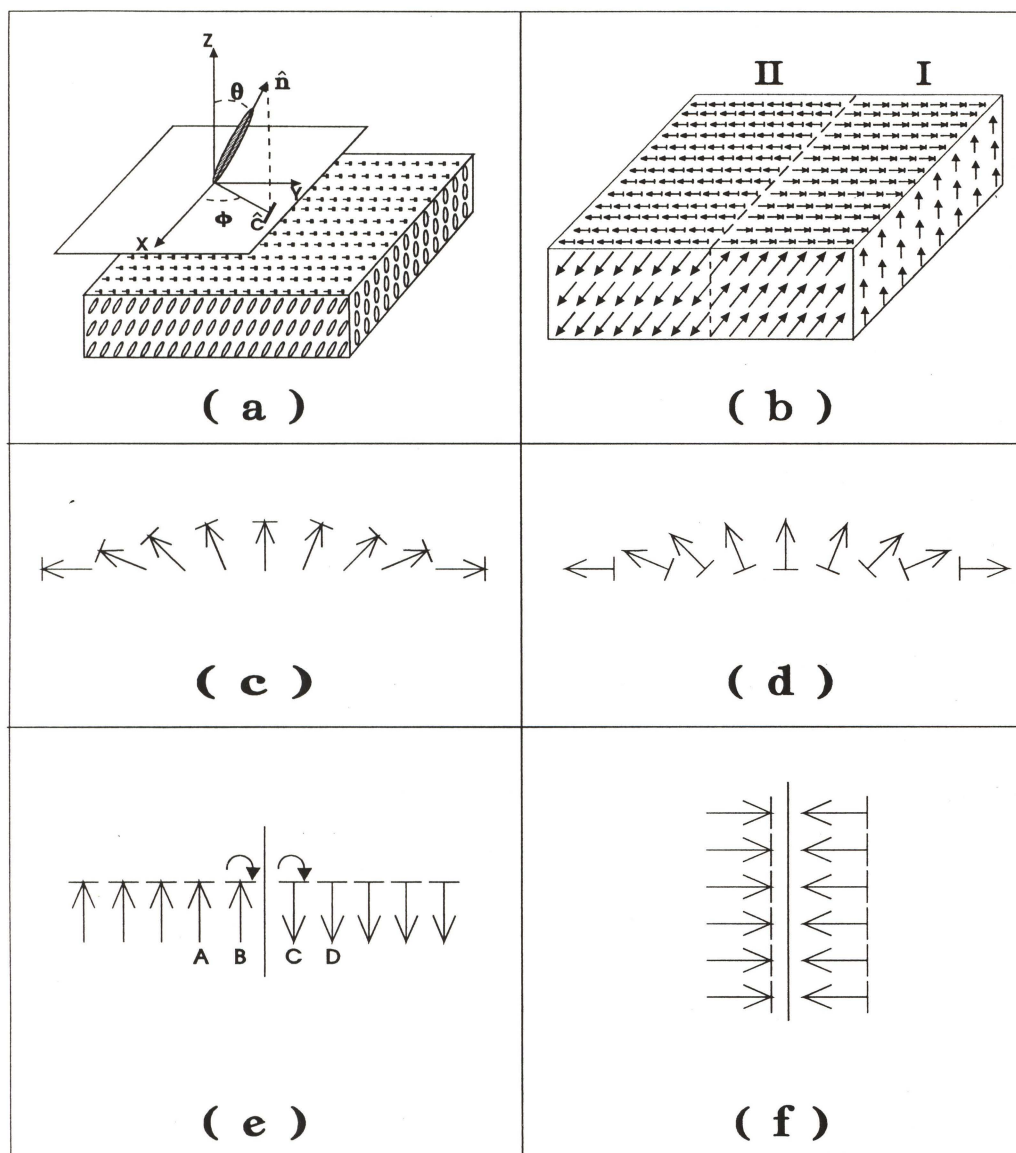


Figure 5.1: (a) Freely suspended smectic-C film geometry. The mean molecular long axis orientation is described by a vector  $\mathbf{n}(\mathbf{r})$  with a fixed tilt angle  $\theta$  from the layer normal. The unit vector called the "c director,"  $\mathbf{c}(x,y)$ , is the projection of  $\mathbf{n}(\mathbf{r})$  on the layer plane and has a variable azimuthal orientation  $\phi(x,y)$ . The "tees" give the projection of  $\mathbf{n}$  on the surfaces indicated, with the small bar distinguishing the end of the molecule closest to the surface. (b) For polar smectic-C films, there are two equivalent states as shown I and II. For the same c-vectors, the underlying polar molecule can be orientated in either direction. (c) The **p**-vector, indicated by the arrow, is a projection of vector  $\mathbf{n}$  onto the layer plane. When the c- vectors and p-vectors are parallel, they have the same signs of splay. (d) When the c-vectors and p-vectors are anti-parallel, they have the opposite signs of splay. (e) If the c-vectors are parallel to the string, then, there is a torque on the string. (f) If the c-vectors are perpendicular to the string, then, there is no torque on the string.



*p*-vector for a 2D film. Suppose the *p*-vector prefers to have positive splay. This corresponds to a *c*-vector with positive splay in phase I [Figure 5.1(c)] and negative splay in phase II [(Figure 5.1(d)]. If a film has both phases, then they share a domain wall which is an “*s*=0 string”. As shown in Figure 5.1(e-f) the orientation of the *c*-vector does not change when crossing a “*s*=0 string”. In order to get a torque free “*s*=0 string”, the *c*-vectors at the boundary always must be perpendicular to the strings. Suppose the *c*-vectors are parallel to a string as shown in Figure 5.1(e). In this case the *c*-vectors of molecules A and B are in the positive splay domain and C and D are in the negative splay domain, thus B tends to rotate clockwise due to its interaction with A, and C also tends to rotate clockwise due to its interaction with D. This instability in the positions of B and C causes them to rotate to positions perpendicular to the string as shown in Figure 5.1(f). The energy of this kind of string is much smaller than that of a surface disclination.

The free energy for such a system can be written as

$$F = \int d^2r \left[ \frac{1}{2} K_s (\nabla \cdot c - pq)^2 + \frac{1}{2} K_b (\nabla \times c)^2 + \epsilon l \right] \quad (5.1)$$

$$= \int d^2r \left[ \frac{1}{2} K_s (\nabla \cdot c)^2 + \frac{1}{2} K_b (\nabla \times c)^2 - \lambda p \nabla \cdot c \right] + \epsilon l + \frac{K_s}{2} q^2. \quad (5.2)$$

Here, *c* is the 2D *c*-vector, *q* is the system's preferred splay strength, and *p* is the polar order parameter which has value of +1, 0 and -1 and changes sign under the operation  $\mathbf{n} \rightarrow -\mathbf{n}$ .  $K_s$  and  $K_b$  are the Frank elastic constants for splay and bend, respectively.  $\lambda \equiv K_s q$  is the coupling constant for the coupling of splay and polar order parameter. Because the coupling term is a total divergence, its integral can be reduced to a surface integral and it will affect the system only when boundaries or domain walls are present. The final term is the string energy for a multiple phase film, where *l* is the length of strings and  $\epsilon$  is the linear energy density of the string. The polar order of a

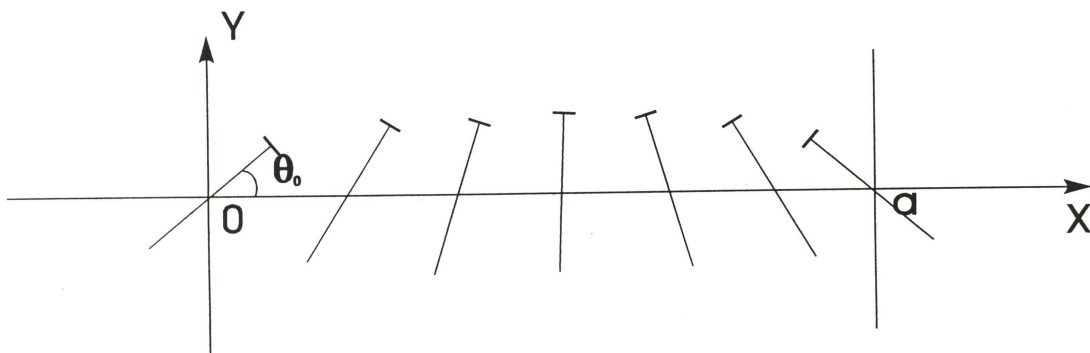


Figure 5.2: The splay stripe geometry.

thin film is often stabilized by impurities on the surface and can be changed by a very slow process of flipping the LC molecules. So once a region of a film is in a polar state, it can stay in that polar state for a very long time. For a single domain film, the stable state is either a uniform polar state or a stripe state with identical stripes only when the system can have surface disclinations at which the angle of the  $c$ -vector changes discontinuously. In the case of multiple phase films, there is a dramatic sequence of phase transitions due to boundary instabilities. The strings only separate domains with different polar symmetries and do not change the continuity of the  $c$ -vectors.

If the stripe is parallel to the  $y$ -axis with width  $a$ ,  $\theta$  changes from  $\theta_0$  to  $\pi - \theta_0$ , and  $p = -1$  as shown in Figure 5.2, then

$$C = (\cos(\theta(x)), \sin(\theta(x))). \quad (5.3)$$

The free energy density of this stripe can be written as

$$f = \frac{K_s}{2} (\sin \theta \cdot \theta_x - q)^2 + \frac{K_b}{2} \cos^2 \theta \cdot \theta_x^2, \quad (5.4)$$

and the Euler equation derived from this free energy is

$$(K_s - K_\delta \cos^2 \theta) \theta_{xx} + K_\delta \cos \theta \sin \theta \cdot \theta_x^2 = 0. \quad (5.5)$$



Here,  $K_\delta \equiv K_s - K_b$  is the difference between the splay and the bend elastic constants. One may notice that this field equation does not depend on  $q$ , the system preferred splay strength.

Using the following substitution,

$$\frac{d^2}{dx^2}\theta = \frac{d\theta}{dx} \cdot \frac{d\theta_x}{d\theta}, \quad (5.6)$$

the field equation can be simplified to

$$(k_s - k_\delta \cos^2 \theta) \frac{d\theta_x}{d\theta} + k_\delta \cos \theta \sin \theta \cdot \theta_x = 0 \quad (5.7)$$

or,

$$\frac{d\theta_x}{\theta_x} = -\frac{k_\delta \cos \theta \sin \theta}{k_s - k_\delta \cos^2 \theta} d\theta = -\frac{1}{2} \frac{d(k_s - k_\delta \cos^2 \theta)}{k_s - k_\delta \cos^2 \theta}. \quad (5.8)$$

. This field equation has the following stripe solution

$$(E(\alpha) - E(\theta_0|\alpha))x = \frac{a}{2}(E(\theta|\alpha) - E(\theta_0|\alpha)). \quad (5.9)$$

Where,  $\alpha = K_\delta/K_s$ ,  $E(\theta|\alpha) = \int_0^\theta \sqrt{1 - \alpha \cos^2 x} dx$  is the second elliptical integral and  $E(\alpha) = E(\pi/2|\alpha)$ . The integration energy of a unit length stripe (disregarding the energy constant) is:

$$E = \frac{2K_s}{a}(E(\alpha) - E(\theta_0|\alpha))^2 - 2K_s q \cos \theta_0 + \epsilon. \quad (5.10)$$

The equilibrium  $\theta_0$  minimizes the above stripe energy. For FSLCFs, the bend elastic constant  $K_b$  is much smaller than the splay elastic constant  $K_s$ , so the value of  $\alpha$  is very close to 1. In this case,

$$\frac{\partial E}{\partial \theta_0} = 2K_s \left( q - \frac{2 \cos \theta_0}{a} \right) \sin \theta_0 = 0, \quad (5.11)$$

and it has solution  $\theta_0 = 0$ , which c-vectors at the stripe boundary perpendicular to the stripe boundary. In all our observations of the splay stripes, the c-directors are perpendicular to or almost perpendicular to the domain walls.

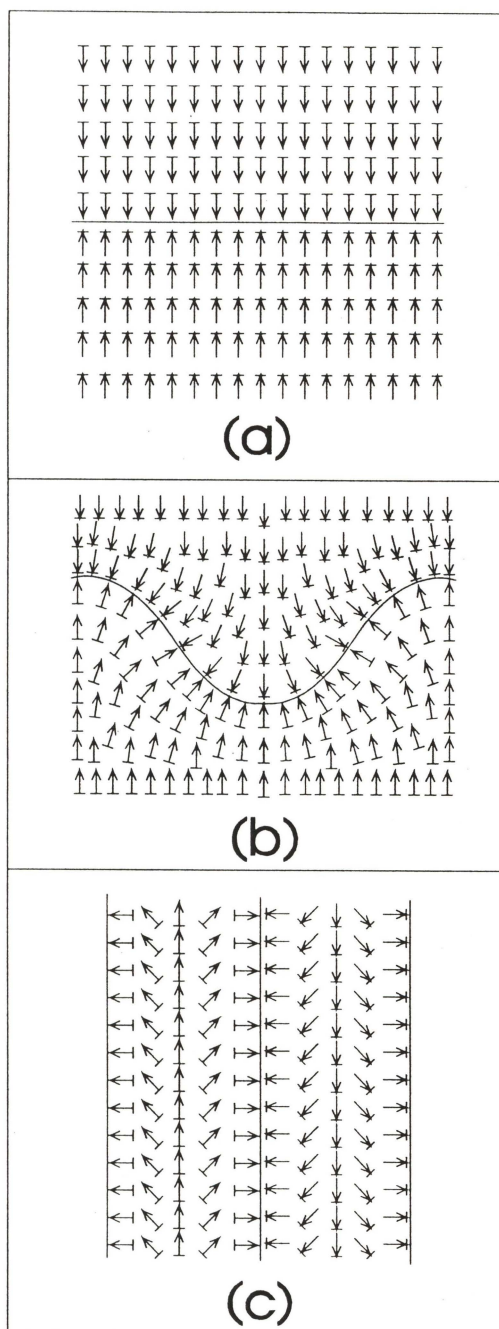


Figure 5.3: The phase transition process of a polar multiple domain smectic-C film. (a) A phase separation phase with a straight string, (b) A critical phase with a sinuous string, or an unstable boundary, (c) A splay stripe phase with an alternation of splay signs between successive stripes.

The equilibrium stripe width,  $a_0$ , minimizes the energy density,  $E/a$ , so

$$a_0 = \frac{4K_s}{2K_s q - \epsilon} = \frac{4K_s}{2\lambda - \epsilon}. \quad (5.12)$$

The stripe width is proportional to the elastic constant and inversely proportional to the coupling constant. The string's linear energy density affects the critical point. In general, the elastic constant is smaller for a thinner film and at higher temperatures, resulting in smaller stripe width. For  $2\lambda < \epsilon$  and  $a_0 < 0$ , the system is in a uniform state with domains separated by straight strings[Figure 5.3(a)]. For  $2\lambda = \epsilon$  and  $a_0 = \infty$ , and the system is in a critical state, that is, the straight string separating the phases are no longer stable, and the strings become sinuous lines[Figure 5.3(b)]. For  $2\lambda > \epsilon$ , the stripe width has a finite value, that is, the amplitude and the period of the sinuous strings are respectively getting larger and tighter as  $\lambda$  increases. Then the whole film turns into a stripe phase[Figure 5.3(c)]. For a film in which the majority of the area is in one polar phase, only the stripe width of the minor polar phase is determined by Equation 5.12 and the total number of stripes is determined by the availability of the minor phase, and the stripe width of majority phase is as wide as possible.

#### 5.4 Experiments and results

Experiments were carried out on 2 to 40 layer thin and uniform FSLCFs of several kinds LC material, 8OSI, DOBAMBC, 7O.7, etc. The bulk materials have isotropic (I), smectic-A (Sm-A), smectic-C(Sm-C) and smectic-I(Sm-I) phases. The chemical formula of the liquid crystal, DOBAMBC and its phase digram are shown in Figure 5.4. Films were drawn over a  $3mm \times 10mm$  hole in a glass cover slip in a hot stage closed with tilted double windows on the top and bottom to minimize internal thermal gradients and give 0.01 K tem-

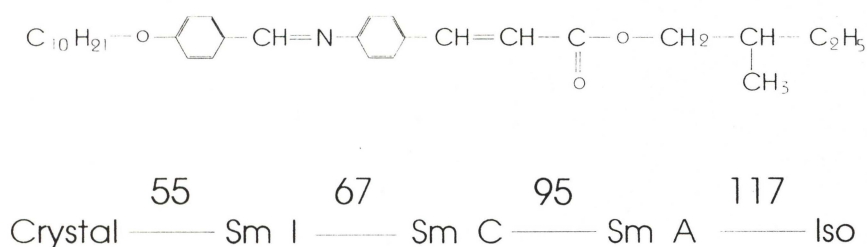


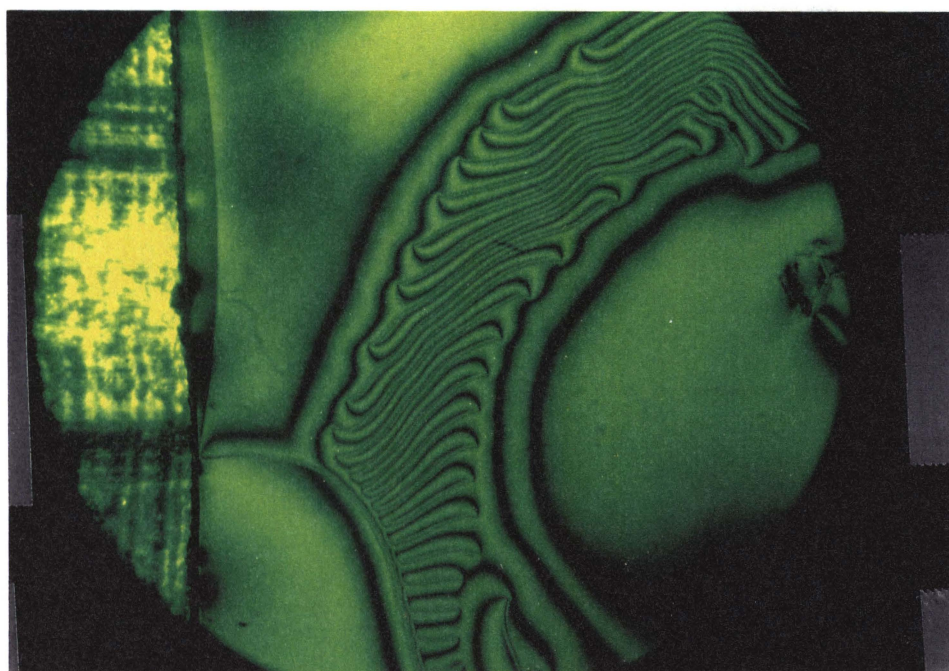
Figure 5.4: The chemical formula and the phase diagram of DOBAMBC.

perature stability. From the DRLM images, we can uniquely map the  $c$ -vector field with the technique described in Chapter II.

Figure 5.5 shows DRLM images of two DOBAMBC films with splay instability. Figure 5.5(a) shows that the left part and right part of the film are in different polar ordering phases and separated by a stripe-like domain wall that was a straight domain wall at lower temperature. Figure 5.5(b) shows a massive splay stripe texture of a 16-layer racemic DOBAMBC film at  $66^\circ\text{C}$ . Figure 5.6 shows a DRLM image of a splay stripe and the underlying pattern of the  $c$ -vector. The domain wall is almost optically invisible here, but it can be shown by the changing brushes. We can uniquely map the  $c$ -vector field from the DRLM image that is shown in Figure 5.6(b).

Figure 5.7 shows a splay instability process for a 40-layer (+)DOBAMBC film with a circular polar domain within which a +1 vortex is trapped at different temperatures. Figure 5.7(a) shows that the polar domain is circular at  $T = 80^\circ\text{C}$ . The four brushes have different intensities indicating the effect of obliquely incident light, and the same reflection intensities of the two sides by the domain wall indicates the  $c$ -vectors are parallel to each other. We can uniquely map the  $c$ -vector field indicating that the  $c$ -vectors have a bend deformation near the vortex center and a splay deformation near the domain





(a)



(b)

Figure 5.4: DRLM images of DOBAMBC films. (a) up image: The left part and right part of the film are in different polar ordering phases and separated by a stripe-like domain wall. (b) low image: Massive splay stripe texture. 16-layer racemic DOBAMBC film at  $66^{\circ}\text{C}$ .

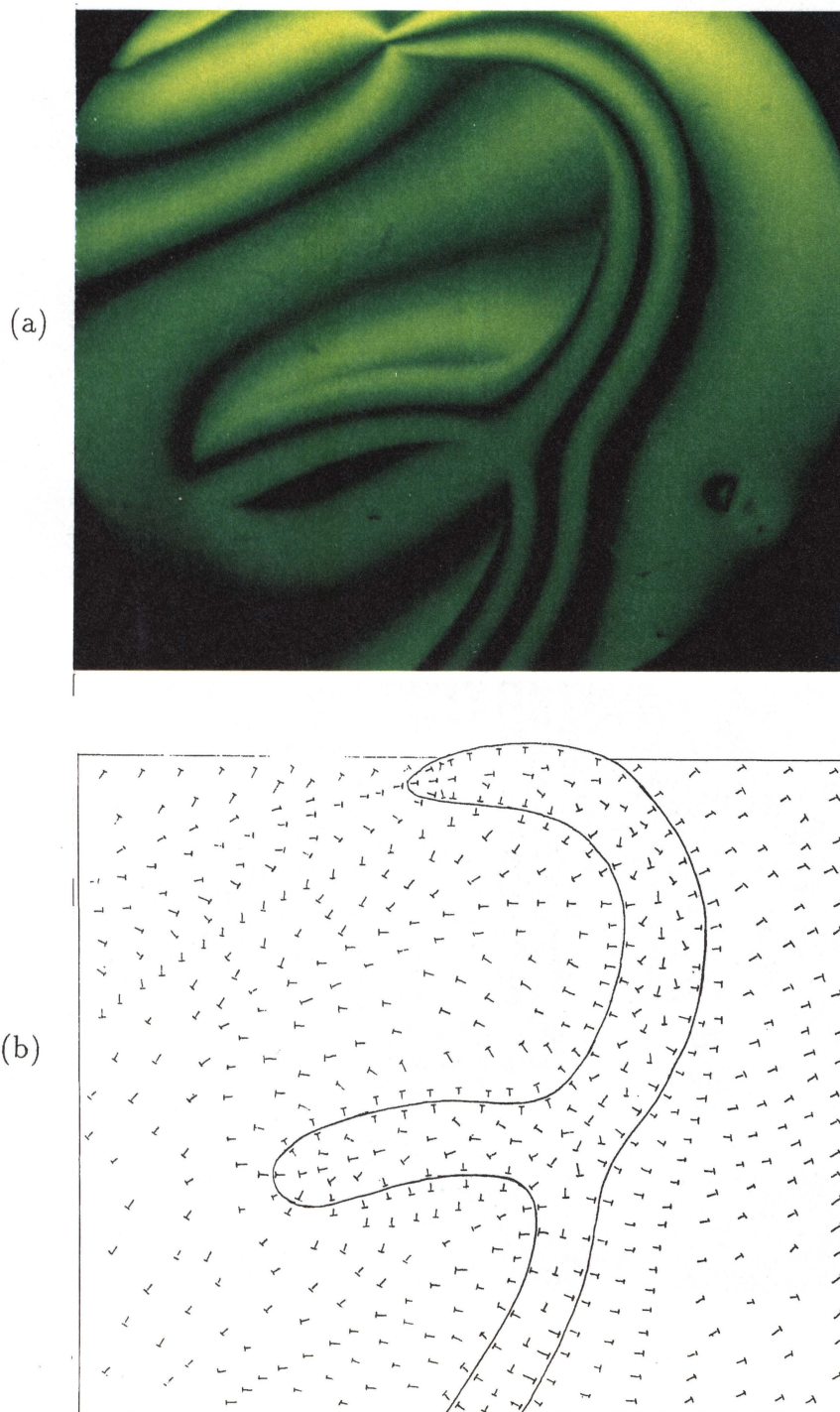


Figure 5.5: DRLM image of a splay stripe (a) and the underlying pattern of c-vector (b).



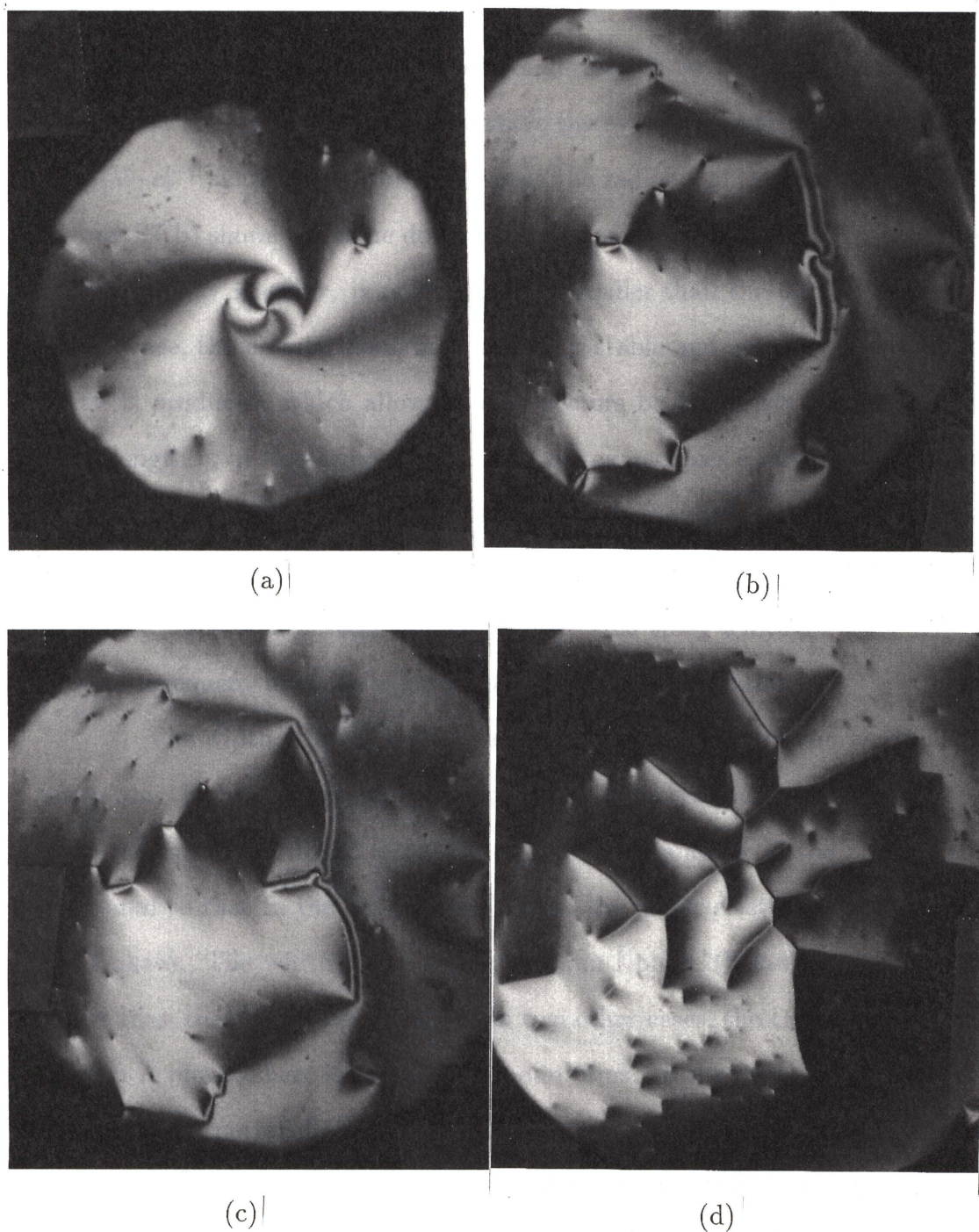


Figure 5.7: DRLM images of the splay instability process of a 40-layer (+)DOBAMBC film with a circular polar domain a +1 vortex is trapped inside at different temperature. (a)  $80^{\circ}\text{C}$ , (b)  $82^{\circ}\text{C}$ , (c)  $85^{\circ}\text{C}$ , and (d)  $110^{\circ}\text{C}$ .

wall; The  $c$ -vectors outside the circular domain change from a splay deformation close to the domain wall to a bend deformation far from the domain wall. The stable circular domain wall indicates the system's preferred splay length  $r_s \equiv |\nabla \cdot c|^{-1}$  at this temperature is about the radius  $r$  of the circular domain. Figure 5.7(b) shows the same domain at temperature  $T = 82^\circ\text{C}$ . The system's preferred splay length  $r_s$  is reduced and is smaller than the domain radius  $r$ . In this case, the circular domain is no longer stable and an elongated domain shape is produced, which allows more  $c$ -vectors be in the system's preferred splay length  $r_s$  at this temperature. The vortex occupies a large area because the  $c$ -vectors near the vortex center cannot be in the preferred splay deformation. Figure 5.7(c) shows that a third arm grows from the center at  $T = 85^\circ\text{C}$  to allow  $c$ -vectors to further reduce the preferred splay length. Figure 5.7(d) shows subsequent branches upon further heating to  $T = 110^\circ\text{C}$ .

The width of splay stripes can be as wide as  $100 \mu\text{m}$  and as small as fewer  $\mu\text{m}$ . Figure 5.8 shows the splay stripe width vs. temperature of a 16-layer racemic DOBAMBC film. The stripe width is larger in the Sm-I phase compared to that in the Sm-C phase due to the larger elastic constant in the Sm-I phase. The width decay rate in the Sm-I phase (below  $67^\circ\text{C}$ ) is much larger than that in the Sm-C phase. In two other cases, the crystal phase and the Sm-A phase, there is no splay stripe in films. In the Sm-A phase, the LC molecules are perpendicular to the film surface, there is no  $c$ -vector and thus no more  $c$ -vector structures. In the crystal phase, the elastic constants are too large to allow any splay stripes in a film.



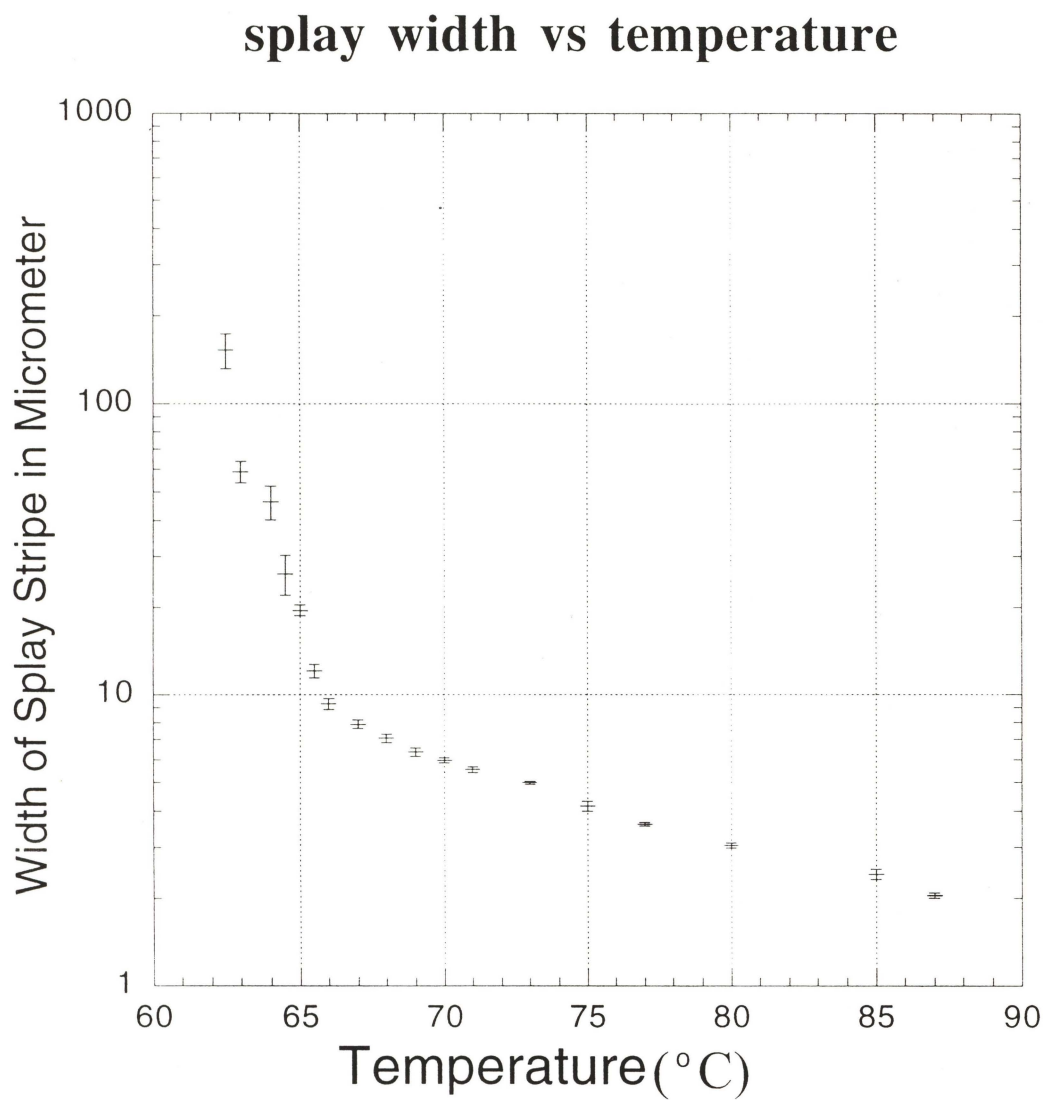


Figure 5.8: The width of splay stripes vs temperature of a 16-layer racemic DOBAMBC film. The phase transition temperature from Sm-I to Sm-C is  $67^{\circ}\text{C}$ .

## CHAPTER VI

### CONCLUSIONS

The study of structural defects and instabilities in freely suspended liquid crystal films has provided new insights into the nature of 2D physics. The results obtained in the present study show that the range of possible phases, structural defects, and instabilities is considerably broader than previously realized.

We have studied three kinds of film structures: normal smectic C films, bilayer films, and polar films. They present different types of symmetry and exhibit different defects and instabilities resulting from spontaneous symmetry breaking.

In normal smectic C films, we are surprised to observe the half-integer and quarter-integer charged vortices. Half-integer charged vortices have been previously observed in nematic phases, but not in smectic phases. Quarter-integer charged vortices have not been observed in any other system. In addition to the observation of the fractionally charged vortices, we have also observed string defects which are attached to vortices or film boundaries. Harmonic functions in the 2D complex plane can be used conveniently to describe string systems.

In bilayer films and polar films, we have discovered two new frustrated phases: the twist-bend stripe phase and the splay stripe phase. In these two cases, the local energetically ideal configurations are the twist-bend or bend deformations, respectively, but these cannot be extended to fill space and must

**Table: Comparison of twist-bend and splay instabilities**

	Twist-bend Instability	Splay Instability
Film Polarity	No	Yes
Layer Polarity	Yes	Yes
Order Parameter	Twist-bend field (changes in space)	Polar Ordering (almost fixed in space)
Uniform Phase	Sm-C	Sm-C with polar separation
Critical Phase	c-vector bend patterns (bulk effect)	sinusoidal strings (boundary effect)
Stripe Phase	Bend stripes	Splay stripes
String structure	c-vectors // string	c-vectors $\perp$ string

Table 6.1: Table: Comparison of twist-bend and splay instabilities.

be accommodated by the appearance of defects, often in periodic arrays. The twist-bend stripe phase is formed in an achiral compound with one aliphatic and one perfluoroalkyl chain and is a novel example of spontaneous chiral-symmetry breaking. This phase transition is mainly driven by the interior twist field generated by the steric interaction of molecules in nonpolar films. The splay stripe phase, on the other hand, arises as a result of a polar ordering phase separation and an instability of the ensuing domain boundaries. The splay and twist-bend instabilities in freely suspended liquid crystal films have some fundamental differences which are summarized in table 6.1.

## Bibliography

- [1] P. G. de Gennes & J. Prost, *The Physics of Liquid Crystals*. (Oxford Science Publications, 2nd ed. 1993.)
- [2] S. Chandrasekhar, *Liquid Crystals*. (Cambridge University Press, 2nd ed., 1992.)
- [3] J. M. Kosterlitz and D. J. Thouless, *J. Phys.* **C6**, 1181(1973).
- [4] G. Freidel, *Les etats mesomorphes de la matiere. Ann. Phys. (paris)* **18**,273(1922).
- [5] R.B. Meyer, *Phys. Rev. Lett.* **22**, 918(1969).
- [6] J. Pang, and N.A. Clark, *Phys. Rev. Lett.* **73**, 2332(1994).
- [7] C.D. Muzny, and N.A. Clark, *Phys. Rev. Lett.* **68**, 804(1992).
- [8] Max Born & Emil Wolf, *Principles of Optics* (Pergamon Press, 6th ed., 1980),P.61.
- [9] C.Y. Young, R. Pindak, N. A. Clark, and R.B. Meyer, *Phys. Rev. Lett.* **40**, 773(1978).
- [10] R. Pindak, C.Y. Young, R.B. Meyer, and N.A. Clark, *Phys. Rev. Lett.* **45**, 1193(1980).
- [11] S.B. Dierker , R. Pindak, and R.B. Meyer, *Phys. Rev. Lett.* **56**, 1819(1986).
- [12] X. Qiu, J. Ruiz-Garcia, K.J. Stine, C.M. Knobler, and J.V. Selinger, *Phys. Rev. Lett.* **67**, 703(1991).
- [13] R.B. Meyer and P.S. Pershan, *Solid St. Comm.* **13**, 989(1973).
- [14] J.E. Maclennan, *Europhys. Lett.* **13**, 435(1990).
- [15] A.M. Levelut, C. Germain, P. Keller, L. Liebert, *J. de Phys.* **44**, 623(1983).
- [16] C.S. Rosenblatt, R. Pindak, R.B. Meyer, and N.A. Clark, *Phys. Rev. A* **21**, 140(1980).
- [17] D.H. Lee and G. Grinstein, *Phys. Rev. Lett.* **55**, 541(1985);
- [18] R.H. Swendsen, *Phys. Rev. Lett.* **49**, 1302(1982);
- [19] R. Hoyst, D.J. Tweet, L.B. Sorensen, *Phys. Rev. Lett.* **65**, 2153(1990);  
D.J. Tweet, R. Hoyst, B.D. Swanson, H. Stragier, and L.B. Sorensen, *Phys. Rev. Lett.* **65**, 2157(1990).



- [20] J.W. Goodby and G.W. Gray, *J. de Phys., Colloq.* **40** C3-27 (1979).
- [21] J.P. Gaughin, J.P. Kelly, G.W. Gray, and J.W. Goodby, *J. de Phys., Colloq.* **40** C3-178 (1979).
- [22] J.M. Carlson, S.A. Langer, and J.P. Sethna, *Europhys. Lett.* **5**, 327 (1988).
- [23] E. Dubois-Violette and B. Pansu, *Mol. Cryst. Liq. Cryst.* **165**, 151(1988); P.P. Crooker, *Liq. Cryst.* **5**, 751(1989).
- [24] J. Ruiz -Garcia, X. Qiu, M.-W. Tsao, G. Marshall, C.M. Knobler, G.A. Overbeck, and D. Mobius, *J. Phys. Chem.* **97**, 6955(1993).
- [25] J.V., in *Complex Fluids*, edited by E.B. Sirota, D. Weitz, T. Witten, and J. Israelchvilli, (Materials Research Society, Pittsburgh, 1992), p. 29.
- [26] N.A. Clark, D. H. Van Winkle, and C.D. Muzny, see S.A. Langer and J.P. Sethna, *Phys. Rev.* **A5**, 5035(1986).
- [27] G.A. Hinshaw, Jr., R.G. Petschek, and R.A. Pelkovitz, *Phys. Rev. Lett.* **60**, 1864(1988).
- [28] J.V. Selinger, Wang, R.F. Bruinsma, and C.M. Knobler, *Phys. Rev. Lett.* **70**, 1139 (1993).
- [29] J. Pang, C.D. Muzny, and N.A. Clark, *Phys. Rev. Lett.* **69**, 2783(1992).
- [30] M. Seul, R. Monar, L. O'Gorman, and R. Wolfe, *Science* **254**, 1616(1991).
- [31] M. Seul and R. Wolfe, *Phys. Rev.* **A46**, 7519(1992); **46**, 7534(1992).
- [32] T.P. Rieker, G.S. Smith, and E.P. Janulis, presented at the Fourth International Conference on Ferroelectric Liquid Crystals, Tokyo, Japan, 1993, P-42.
- [33] J. Hopken and M. Moller, *Macromol.* **25**, 2482(1992).
- [34] J. Pang and N.A. Clark, to be published. These results were obtained from studies of the dynamics of single layer islands and holes in films of various thickness.
- [35] *Polymer Handbook*, edited by J. Brandup and E.H. Immergut. J. Wiley and Sons, New York, 1975.
- [36] I. Szleifer, A Ben-Shaul and W.M. Gelbart, *J. Chem. Phys.* **85**, 5345(1986).
- [37] J.V. Selinger and R.L.B. Selinger, *Phys. Rev.* **E51**, ??(1995).
- [38] M. Seul and D. Andelman, *Science*, **267**, 476(1995).
- [39] F.C. Frank, *Disc. Faraday Soc.* **25**, 19(1958).
- [40] R. Williams, *Advan. Chem. Ser.* **63**, 61(1967); G. H. Heilmeyer, *ibid.* **63**, 68(1967).





